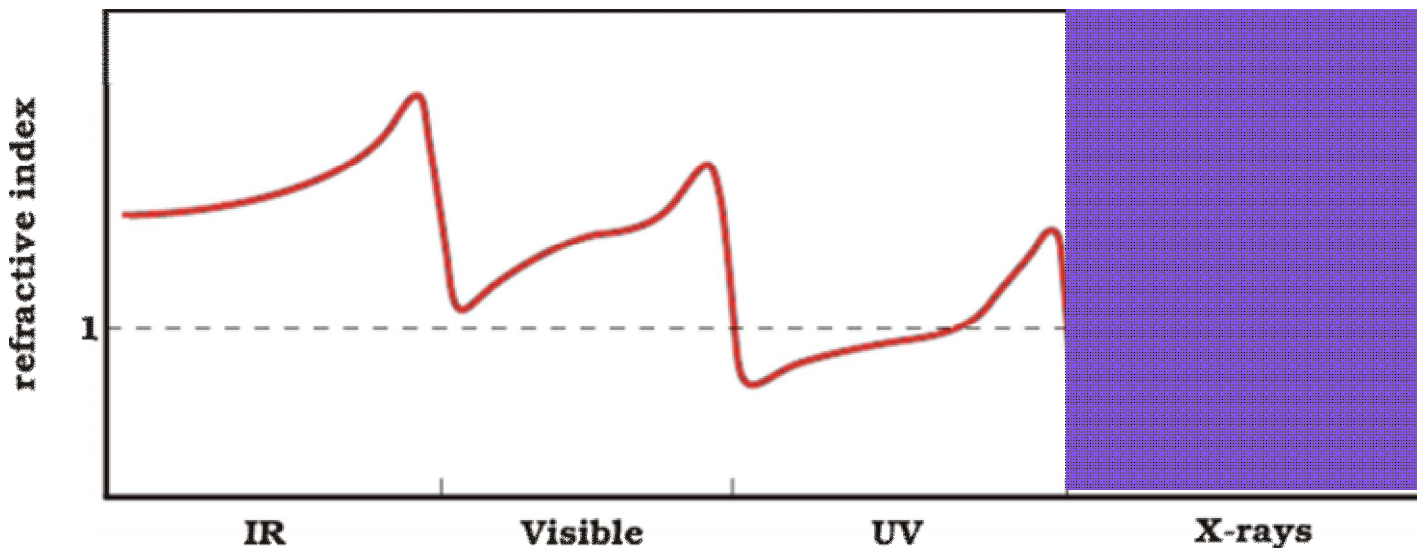


Confocal Microscopy for 3D elemental imaging and Analysis

Andreas Karydas,
Nuclear Spectrometry and Applications Laboratory
IAEA Laboratories, Seibersdorf
A.Karydas@iaea.org

X-rays Optics

Refractive index $\Rightarrow n = \frac{c}{u_p}$



$$n = 1 - \delta - i\beta$$

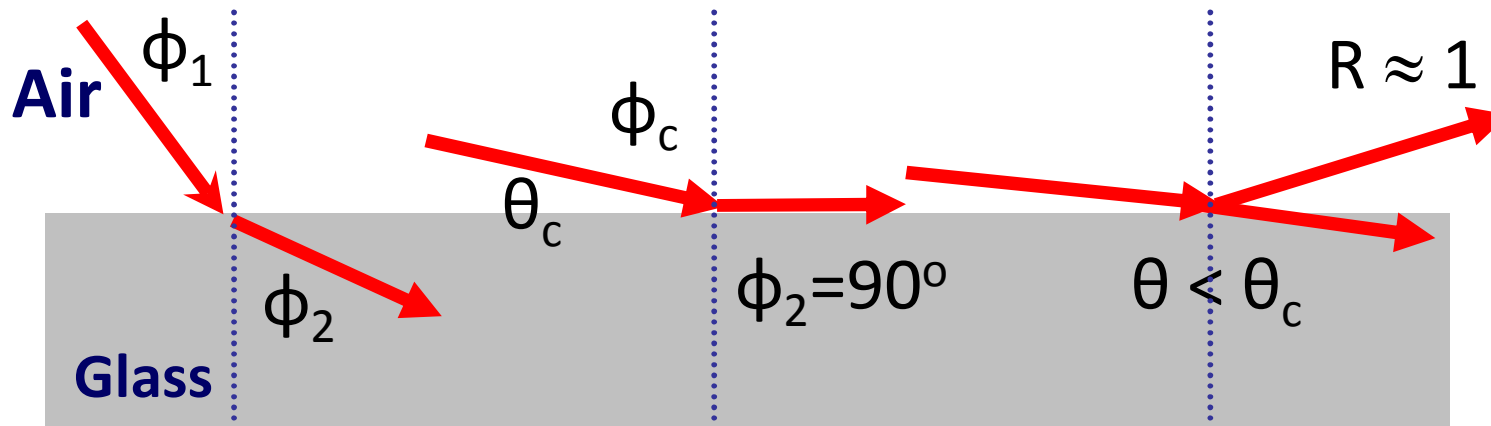
$$\delta = \frac{414.7}{E^2} \cdot \frac{Z_\rho \cdot \rho}{A}$$

phase term

$$\beta = \frac{\lambda}{4\pi} \tau$$

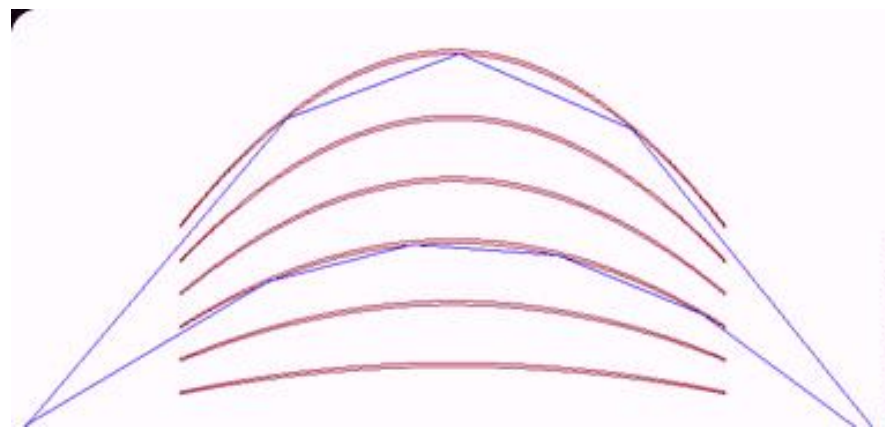
attenuation term

X-Ray optics: External total reflection



Snell Law: $\sin \varphi_2 = \frac{\sin \varphi_1}{n} \Rightarrow \varphi_2 > \varphi_1$

$$\theta_c = \sqrt{2\delta} = \frac{28.8}{E} \cdot \sqrt{\frac{Z_\rho \cdot \rho}{A}}$$

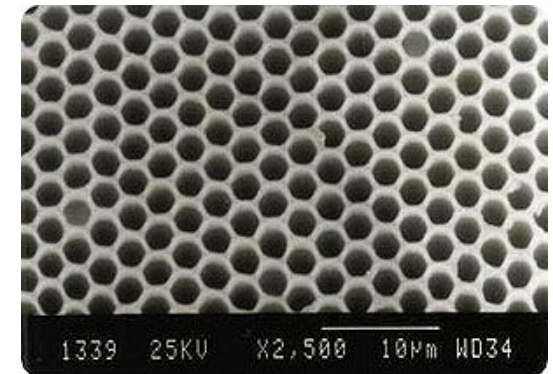
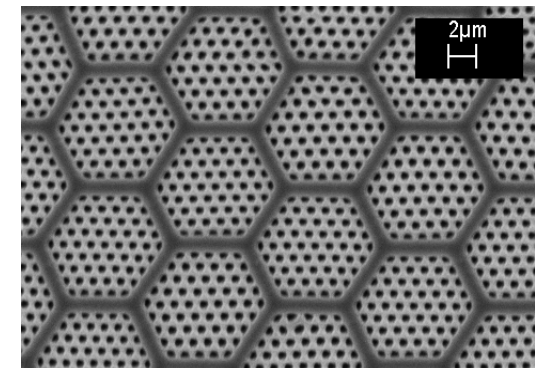
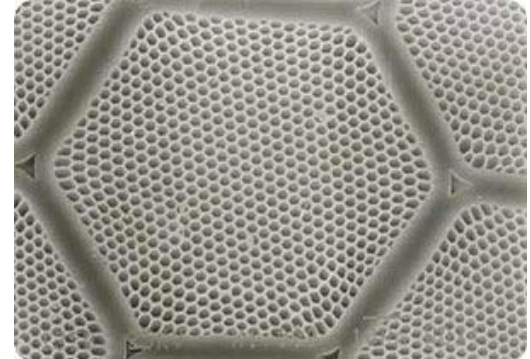


θ_c in the mrad range

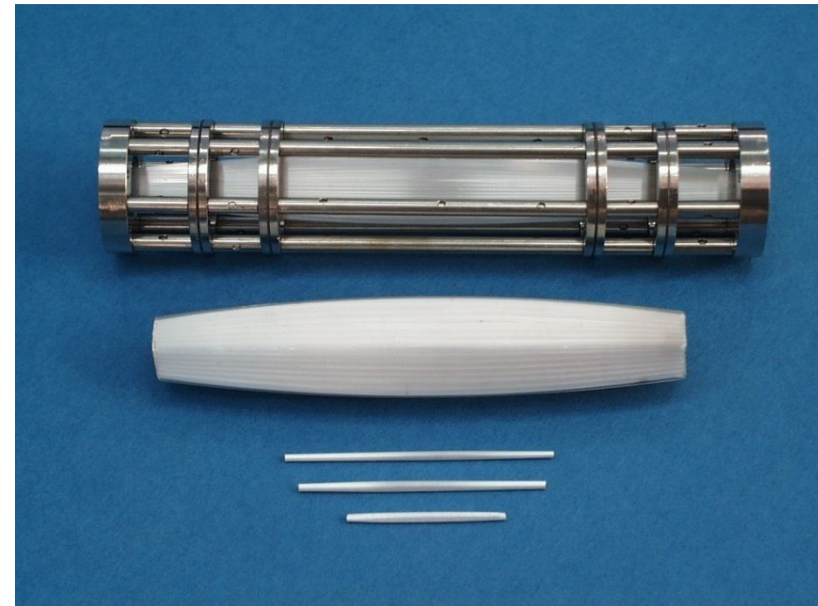
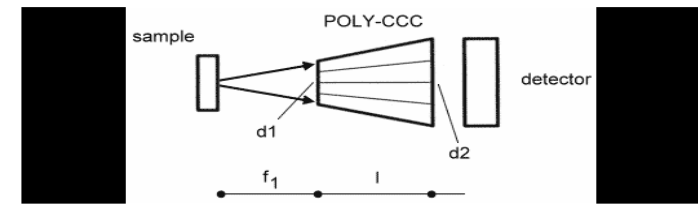
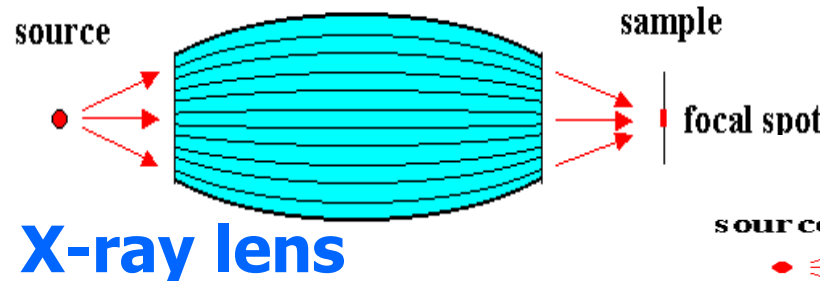
Polycapillary X-ray lenses

Bundles of thousands glass mono-capillaries:

- Directing
- Focusing
- Parallelizing



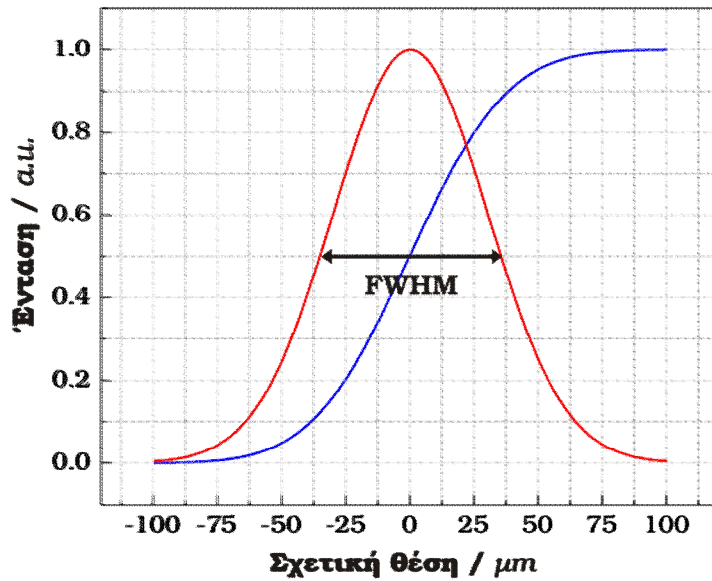
Characteristics of X-Ray lenses



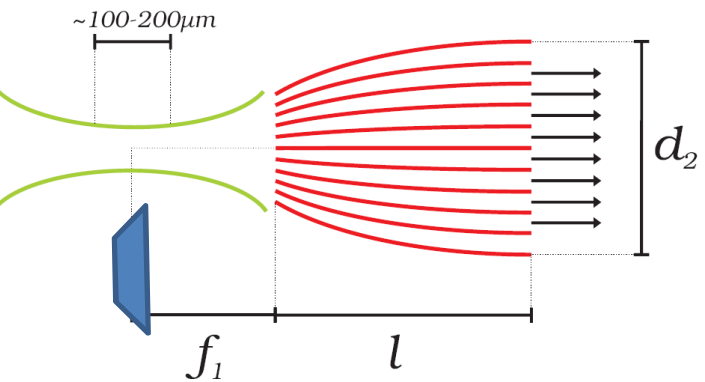
Characteristics of polycapillary X-ray lenses

Important lens parameters:

- **Focal distance** (few mm).
- **Size of the focal region** represented by the FWHM of a Gaussian intensity distribution (down to $\sim 12 \text{ }\mu\text{m}$ @ CuK α)
- **Transmission efficiency**

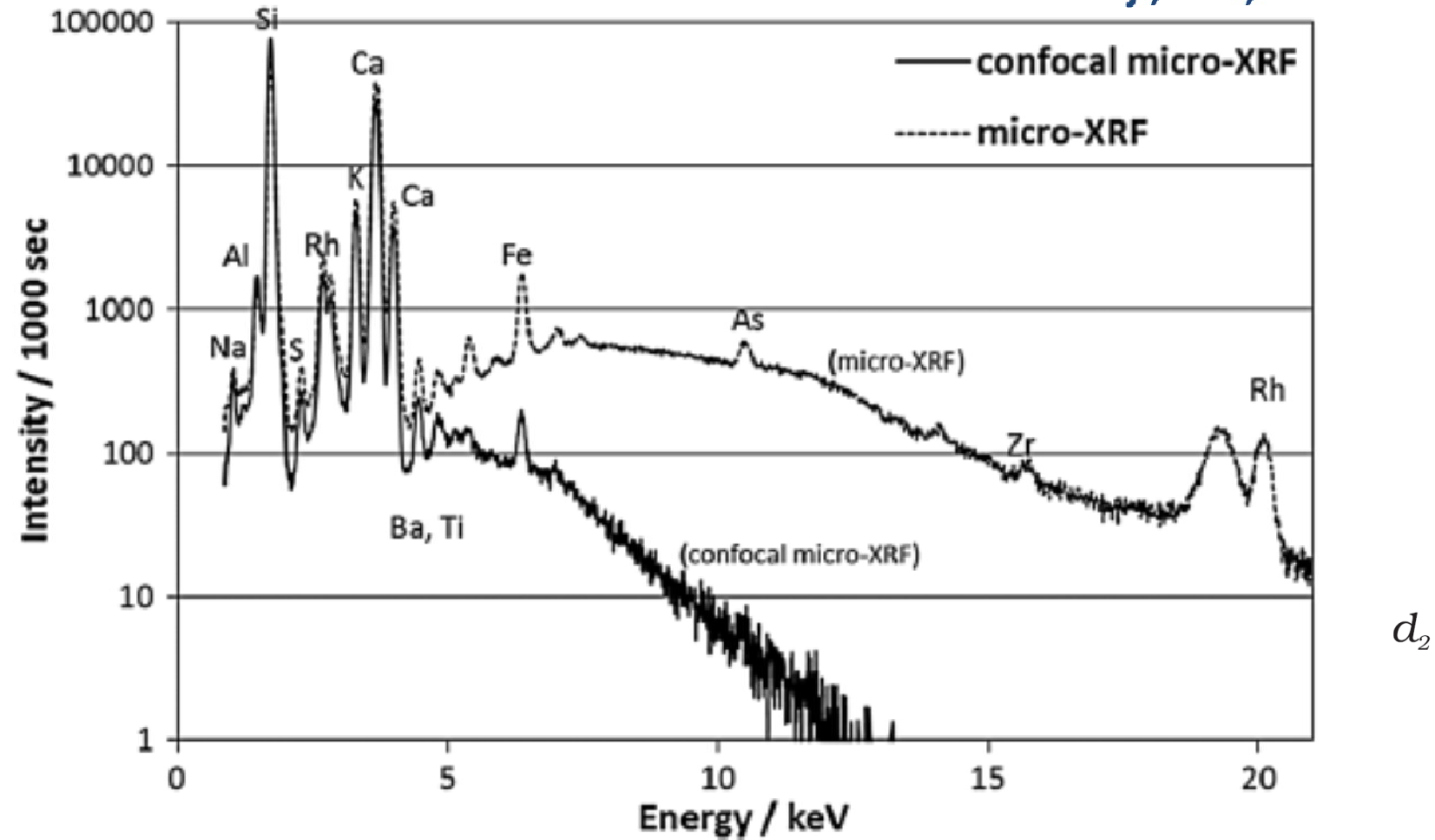


Knife edge scan



Characteristics of polycapillary X-ray lenses

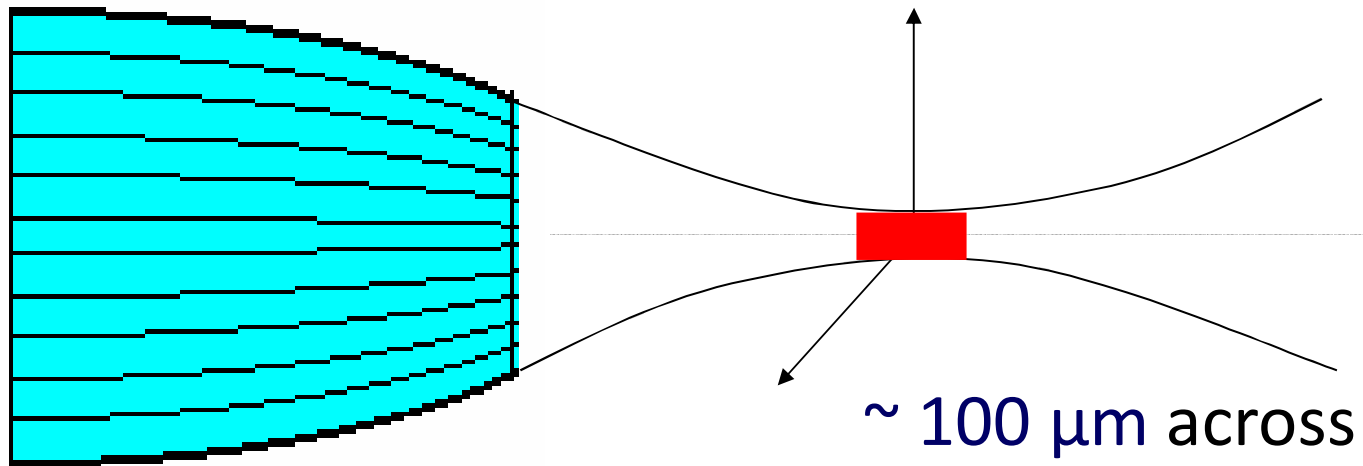
Nakazawa and Tsuji, XRS, 2013



d_2

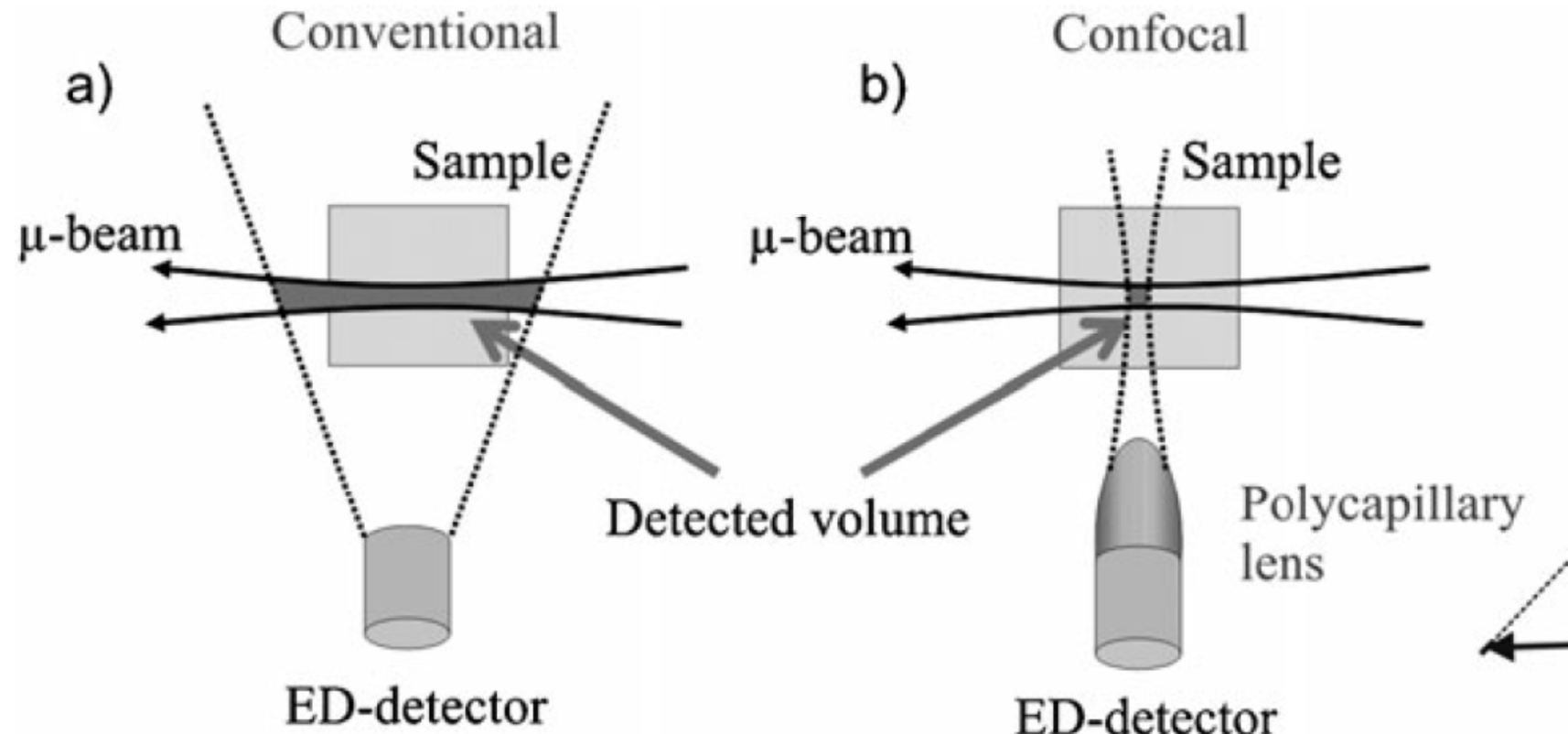
X-Ray lens spatial resolution

Plane vertical to the optical axis:
Two dimensional Gaussian



~ 100 μm across the
optical axis and the focal
plane of the lens the spatial
resolution remains constant

PIXE-XRF: Conventional vs Confocal Geometry

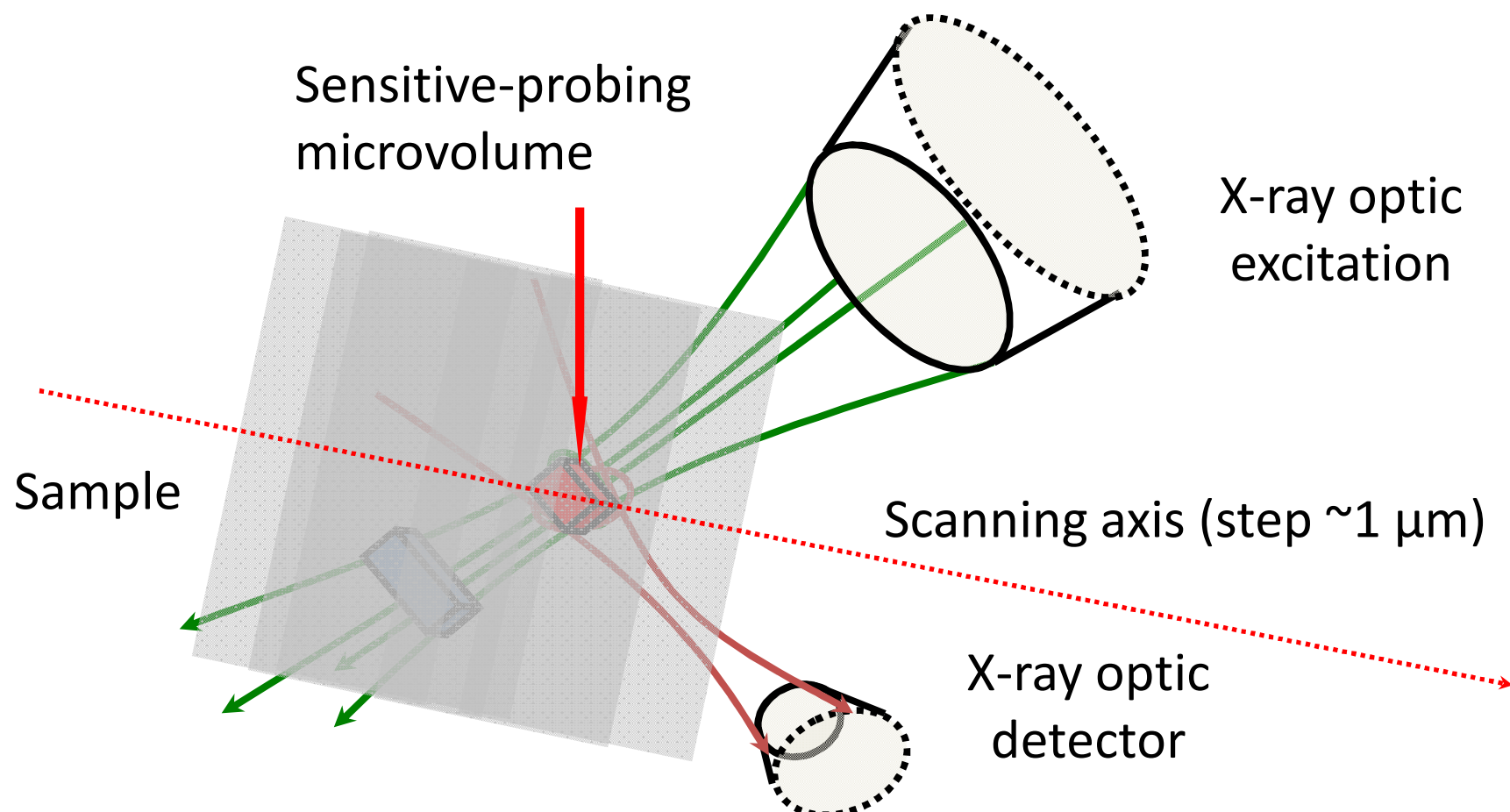


Silversmit et al, Phys. Chem. Phys. Chem. 12 (2010) 5653

Principle of Confocal X-ray analysis

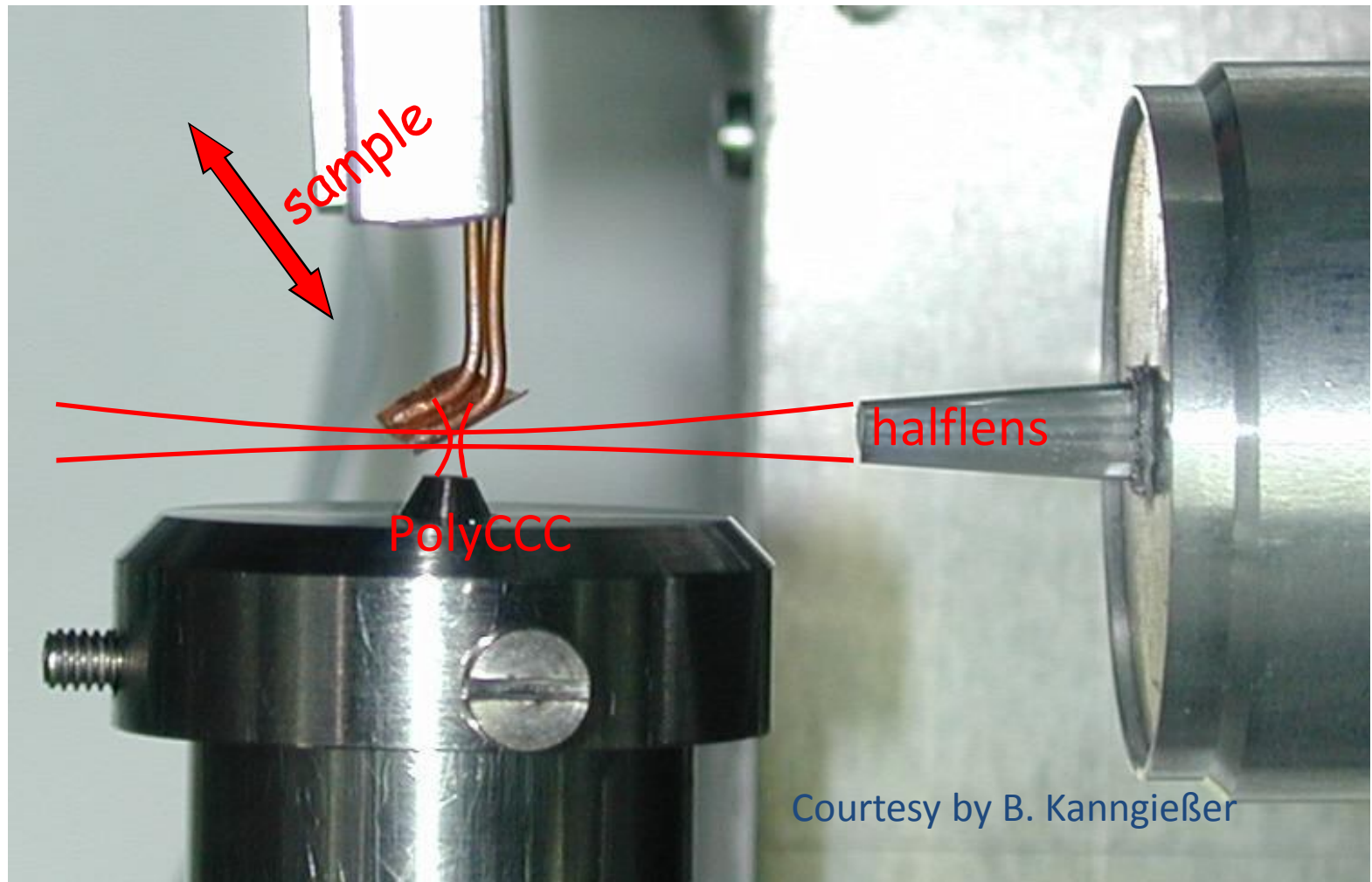
B. Kanngießer, I. Reiche, W.
Malzer, NIM B 211, 2003

confocal setup

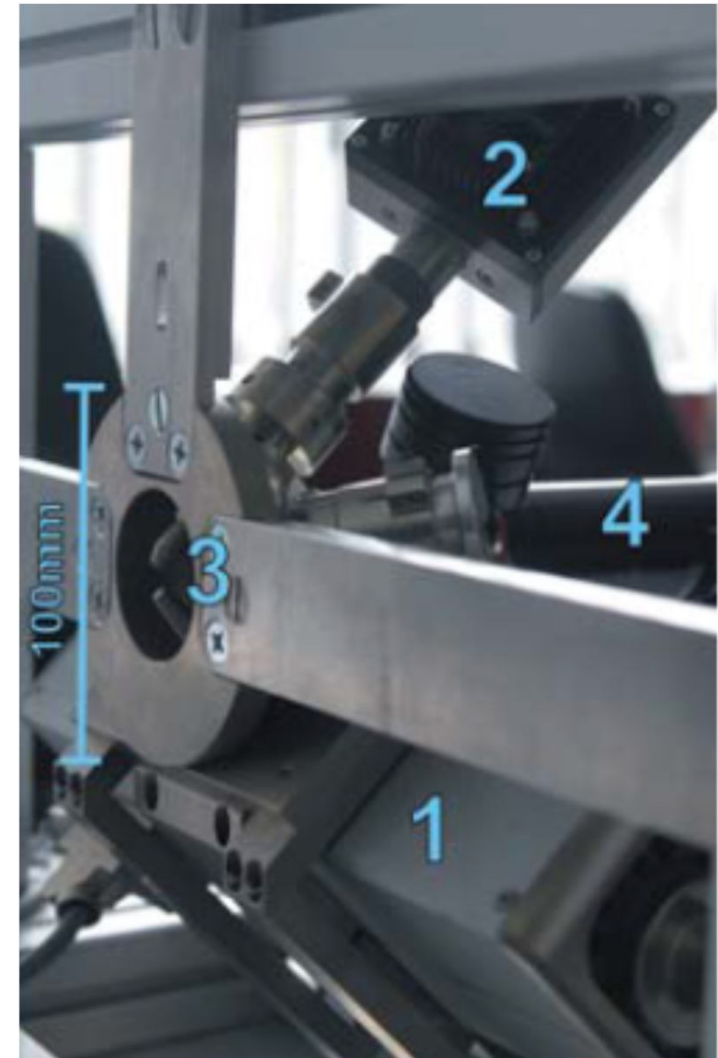
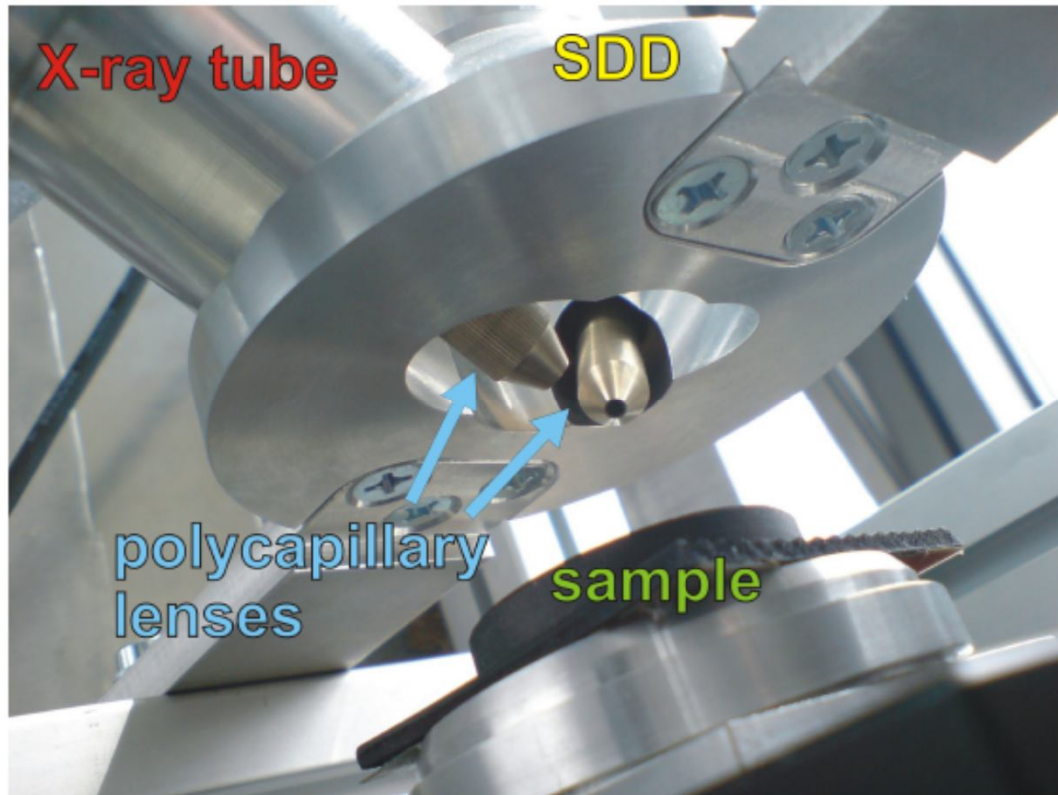


3D Micro XRF Spectrometry:

First setup of the 3D Micro-XRF, @ BAMline, BESSY



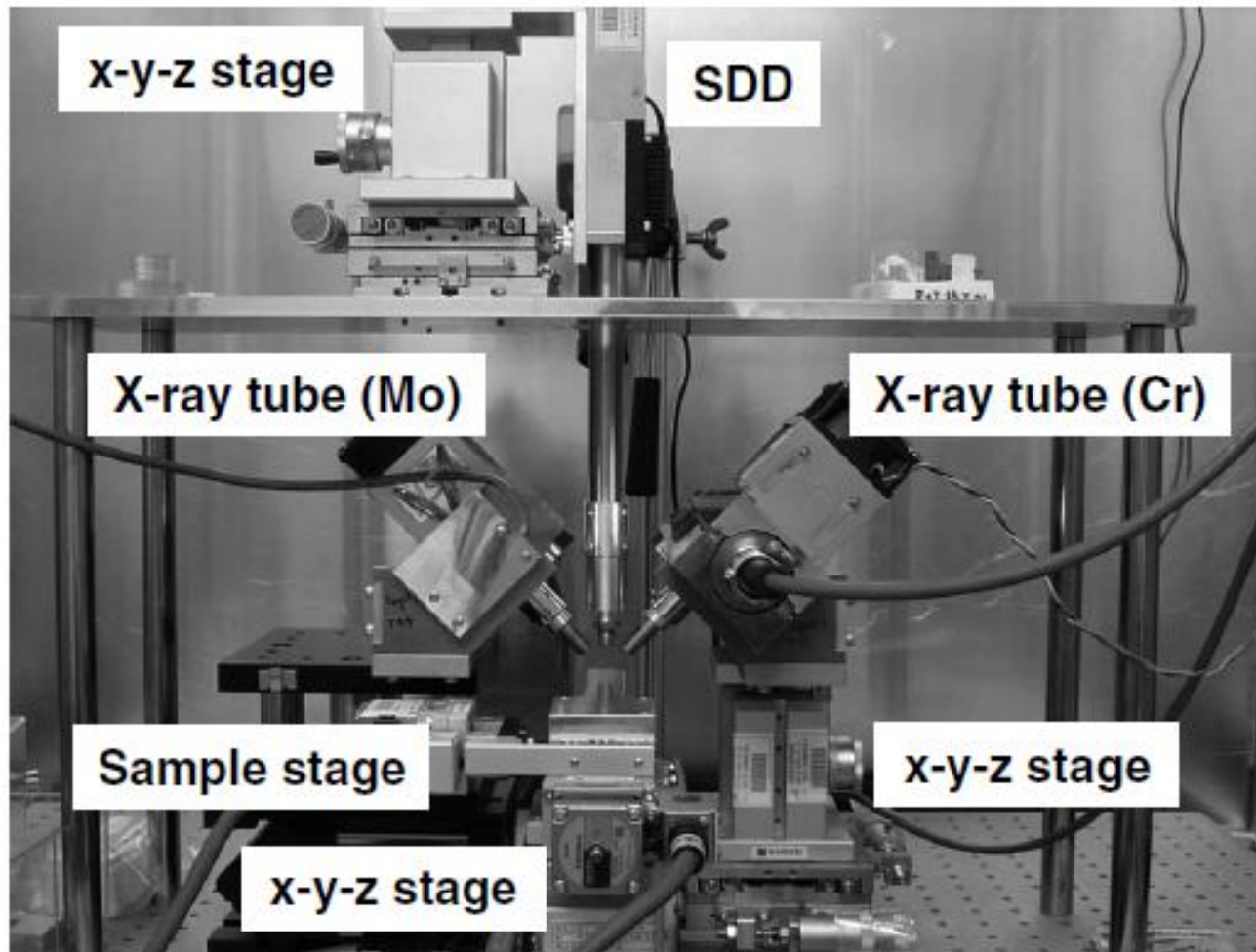
3D Micro-XRF setup @ TU Berlin



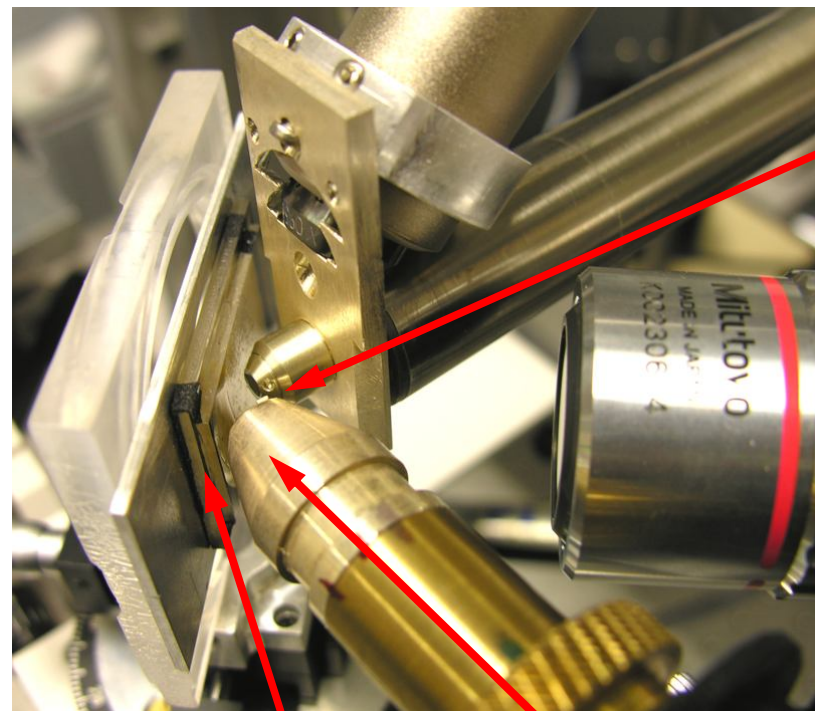
I. Mantouvalou et al., J. Anal. At. Spectrom., 2010, 25, 554–561

Osaka City University, Japan

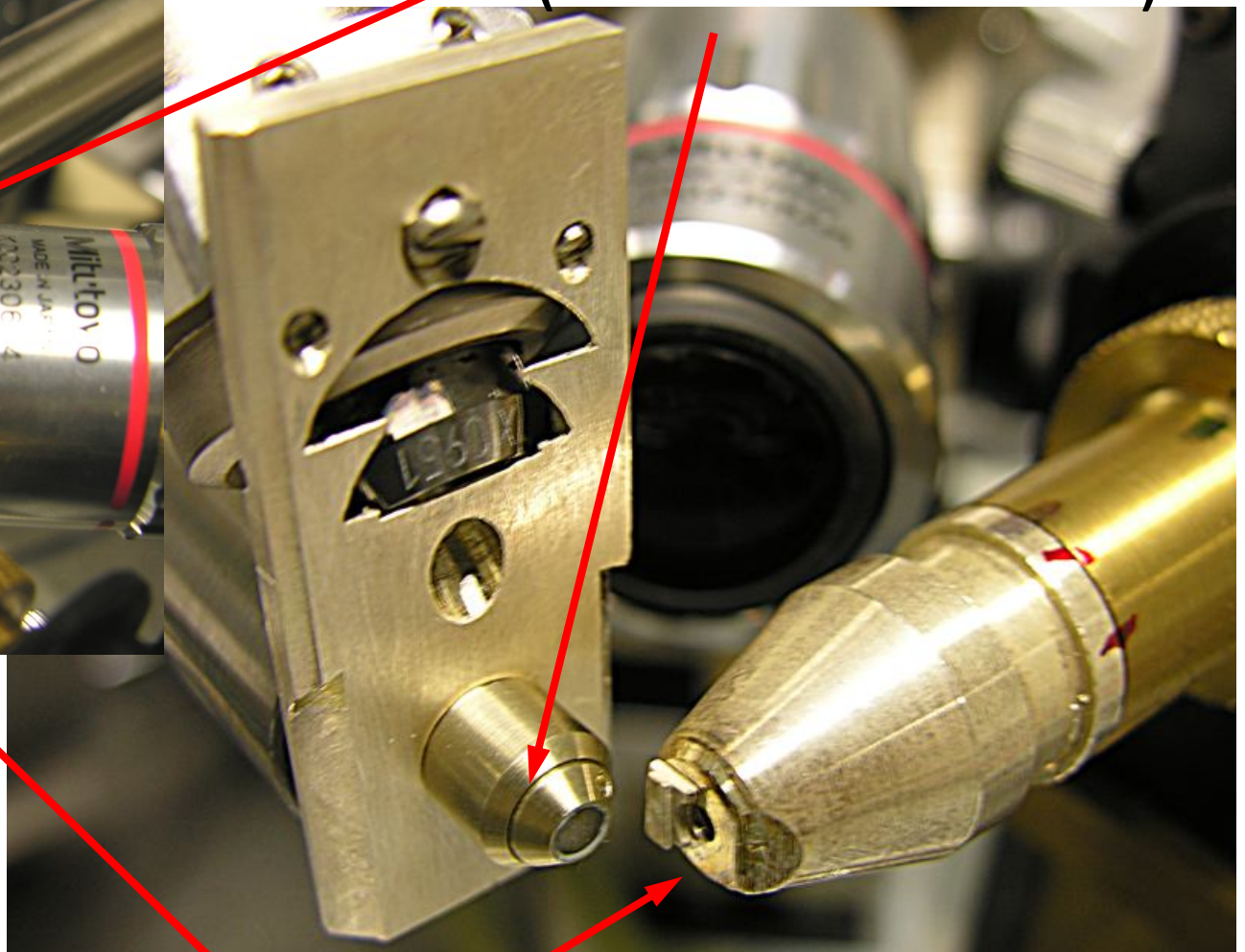
Tsuji and Nakano, XRS (2007), 36, 145



3D uXRF set-up @IAEA



sample in
measuring
position

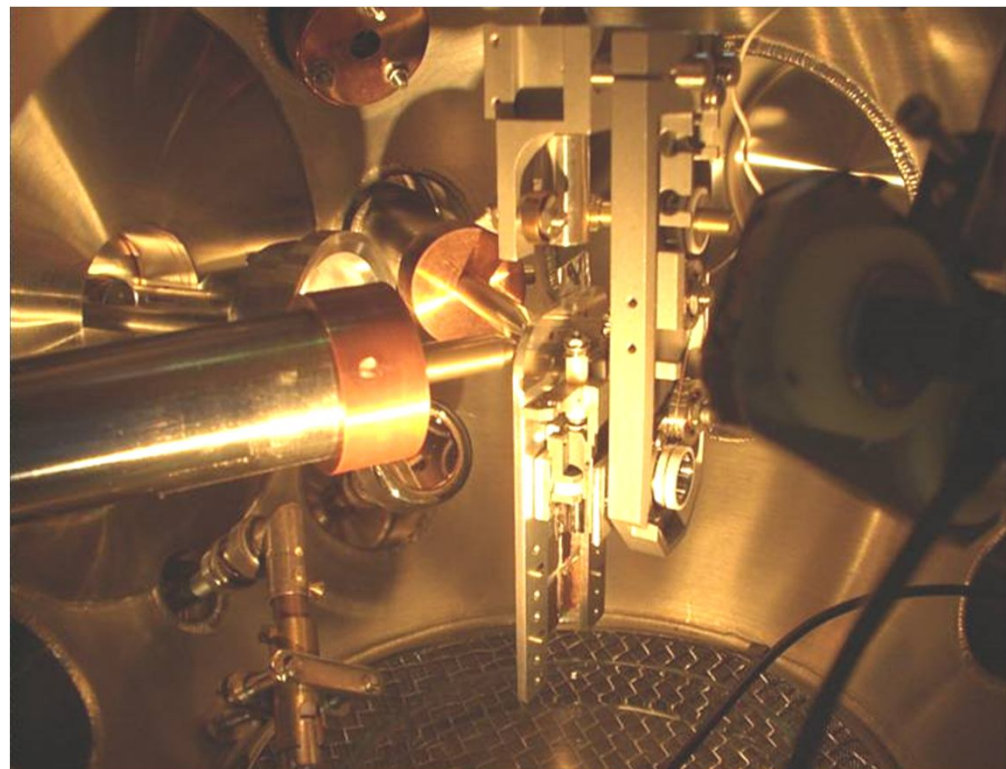
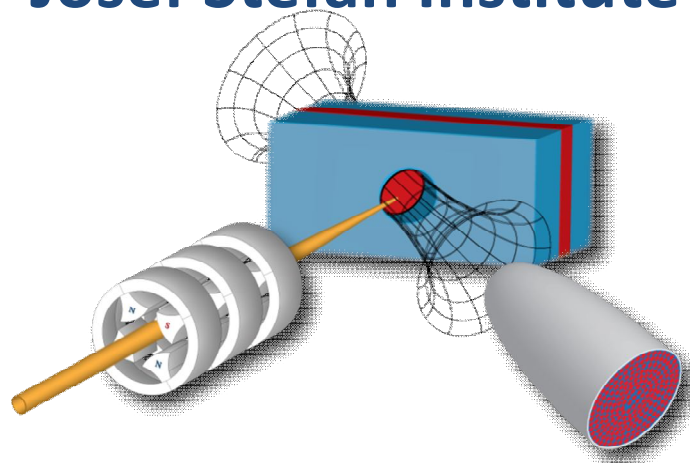


polyCCC
(confocal detector)

polycapillary (primary beam)

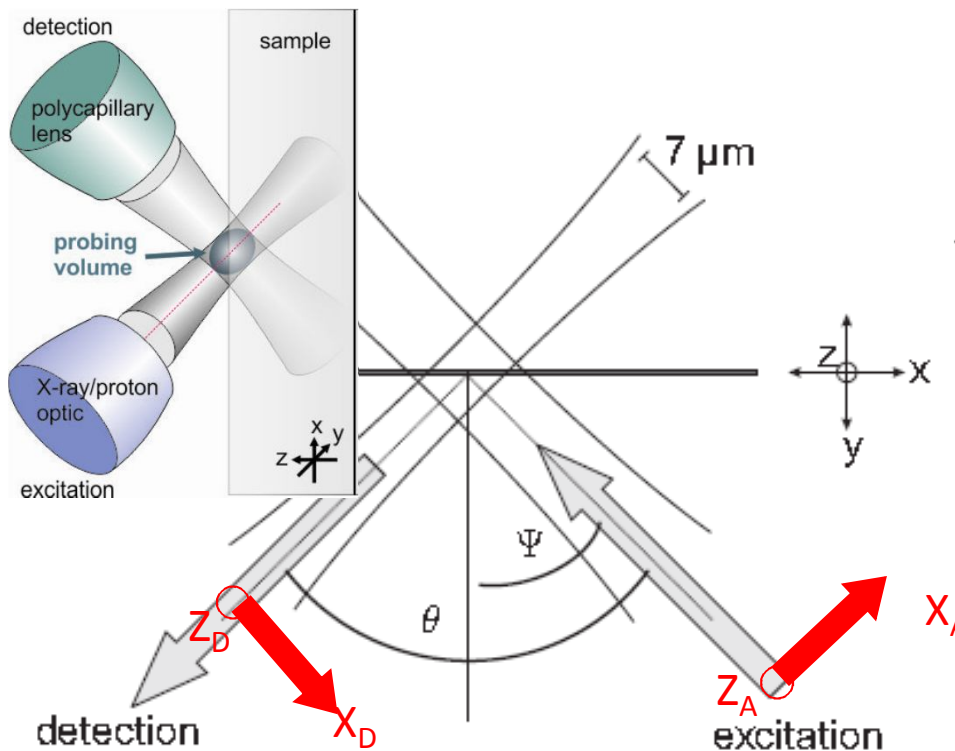
3D Micro-PIXE SET-UP, 2007 @

Josef Stefan Institute Micro-Analytical Center, Ljubljana



Karydas et al, JAAS 2007

Quantification in Confocal Micro XRF (1)



3D set-up sensitivity
for the detection of
specific fluorescence lines

The shape has a three
dimensional ellipsoid



IAEA

A.G. Ka

Intensity distribution for the exciting x-ray beam:

$$\eta_A = \frac{T_A}{2\pi\sigma_A^2} \exp\left(-\frac{x_A^2 + z_A^2}{2\sigma_A^2}\right)$$

Coordination system attached to the excitation lens

T_A, T_B : Lens transmission

σ_A, σ_B : Spot size

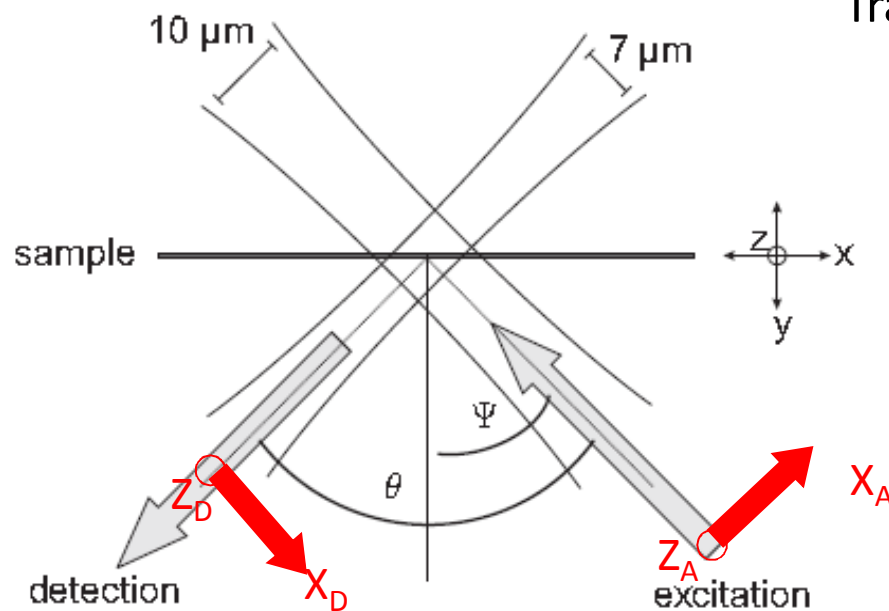
Ω : solid angle

Coordination system attached to the detection lens

$$\eta_D = \frac{\Omega T_D}{4\pi} \exp\left(-\frac{x_D^2 + z_D^2}{2\sigma_D^2}\right)$$

$$\begin{aligned} \hat{\eta}(x, y, z) &= \eta_A \eta_D \epsilon \\ &= \frac{\Omega T_A T_D \epsilon}{8\pi^2 \sigma_A^2} \exp\left(-\frac{\sigma_D^2 x_A^2 + \sigma_A^2 x_D^2 + (\sigma_D^2 + \sigma_A^2) z^2}{2\sigma_A^2 \sigma_D^2}\right) \end{aligned}$$

Quantification in Confocal Micro XRF (2)



Transformation to the sample coordinate system

$$x_A = x \sin(\Psi) + y \cos(\Psi)$$

$$x_D = x \cos(\Psi) - y \sin(\Psi)$$

$$z_A = z_D = z$$

$$\tilde{\eta}(y) = \int_{-\infty}^{\infty} \int_{-\infty}^{\infty} \hat{\eta}(x, y, z) dx dz$$

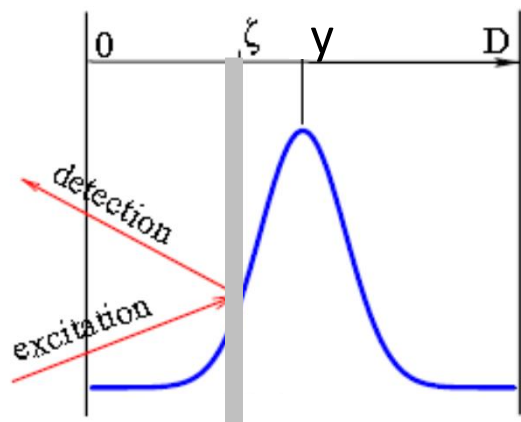
$$= \frac{\Omega T_A T_D \epsilon}{4\pi} \frac{\sigma_D^2}{\sqrt{(\sigma_D^2 + \sigma_A^2)(\cos^2(\Psi)\sigma_A^2 + \sin^2(\Psi)\sigma_D^2)}} \exp\left(-\frac{1}{2} \frac{y^2}{(\sin^2(\Psi)\sigma_D^2 + \cos^2(\Psi)\sigma_A^2)}\right)$$

Mantouvalou, PhD Thesis, Berlin 2009
 Maltzer, kanngiesser, SAB 60 (2005) 1334 – 1341

$$= \frac{\eta}{\sqrt{2\pi}\sigma_y} \exp\left(-\frac{y^2}{2\sigma_y^2}\right)$$

Quantification in Confocal Micro XRF (3)

Fluorescence intensity in confocal geometry for an homogeneous sample



$$\Phi_i(y) = \Phi_o \cdot \sigma_{F,i} \int_0^D \bar{\eta}_i(\zeta - y) \rho_i(\zeta) \cdot \exp(-\bar{\mu}_{lin,i}\zeta) \cdot d\zeta$$

Local density of element *i*

$$\begin{aligned} \bar{\mu}_{lin,i} &= \bar{\mu}_i \cdot \rho = \left(\sum_{elements j} \left(\frac{\mu_{0,j}}{\cos(\theta_A)} + \frac{\mu_{i,j}}{\cos(\theta_D)} \right) w_j \right) \rho \\ &= \sum_{elements j} \left(\frac{\mu_{0,j}}{\cos(\theta_A)} + \frac{\mu_{i,j}}{\cos(\theta_D)} \right) \rho_j \end{aligned}$$

$$\Phi_i(y) = \frac{\Phi_o \cdot \eta_i \cdot \rho_i \cdot \sigma_{F,i}}{2} \times \exp\left(-\frac{(\bar{\mu}_{lin,i} \sigma_{y,i})^2}{2}\right) \times \exp(-\bar{\mu}_{lin,i} y) \times$$

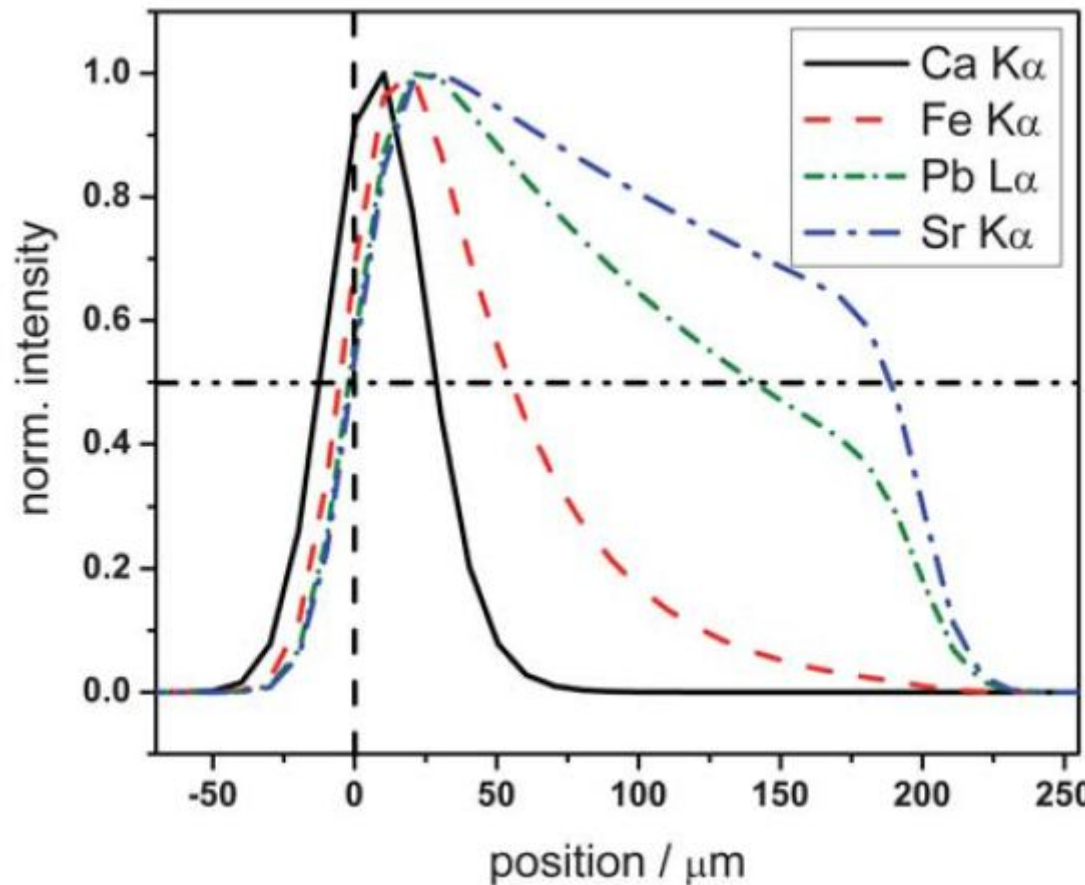
$$\times \left[\operatorname{erf}\left(\frac{D + \bar{\mu}_{lin,i} \sigma_{y,i}^2 - y}{\sqrt{2} \sigma_{y,i}}\right) - \operatorname{erf}\left(\frac{\bar{\mu}_{lin,i} \sigma_{y,i}^2 - y}{\sqrt{2} \sigma_{y,i}}\right) \right]$$

corrects for the actual extension of the probing volume

stands for the decrease of the intensity at probing depth *x* due to absorption.

important if the probing volume intersects the layer boundaries.

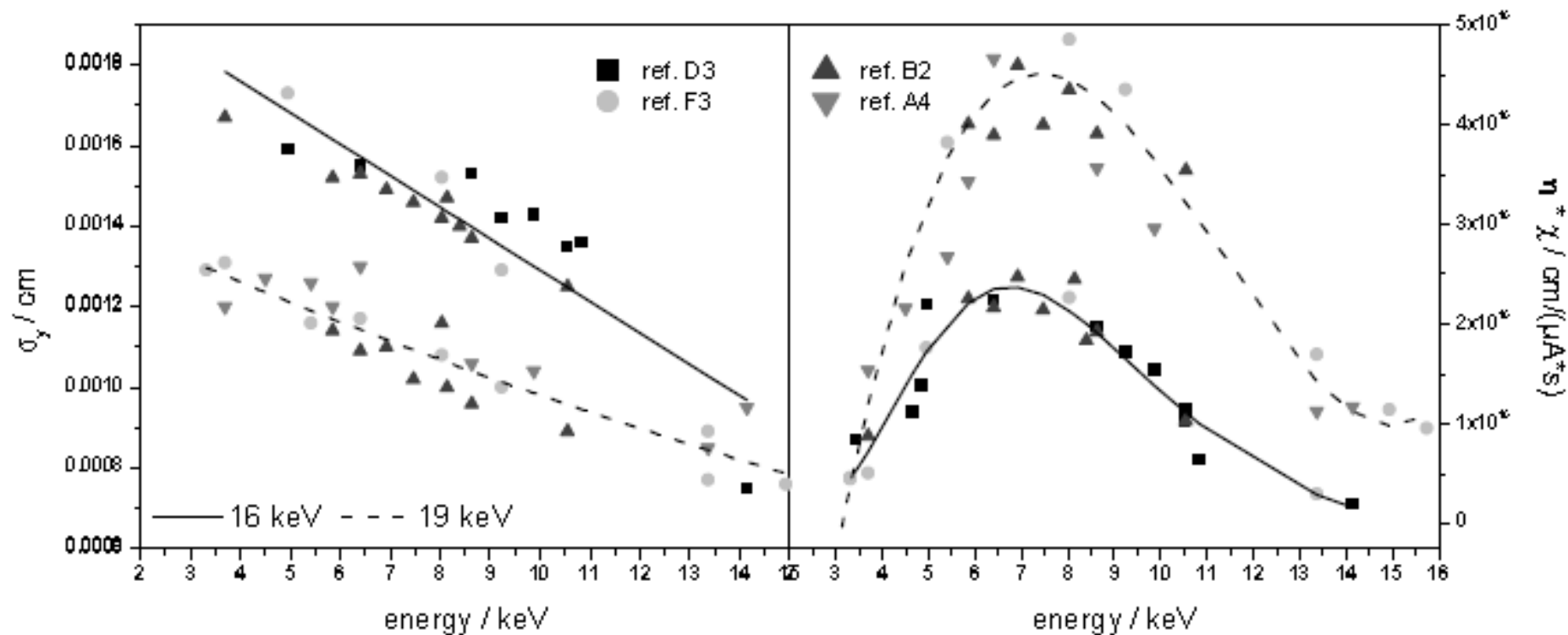
Shape of intensity profiles versus depth



SiO_2 matrix, similar concentration (50 ppm), 19 keV excitation

I. Mantouvalou et al., J. Anal. At. Spectrom., 2010, 25, 554–561

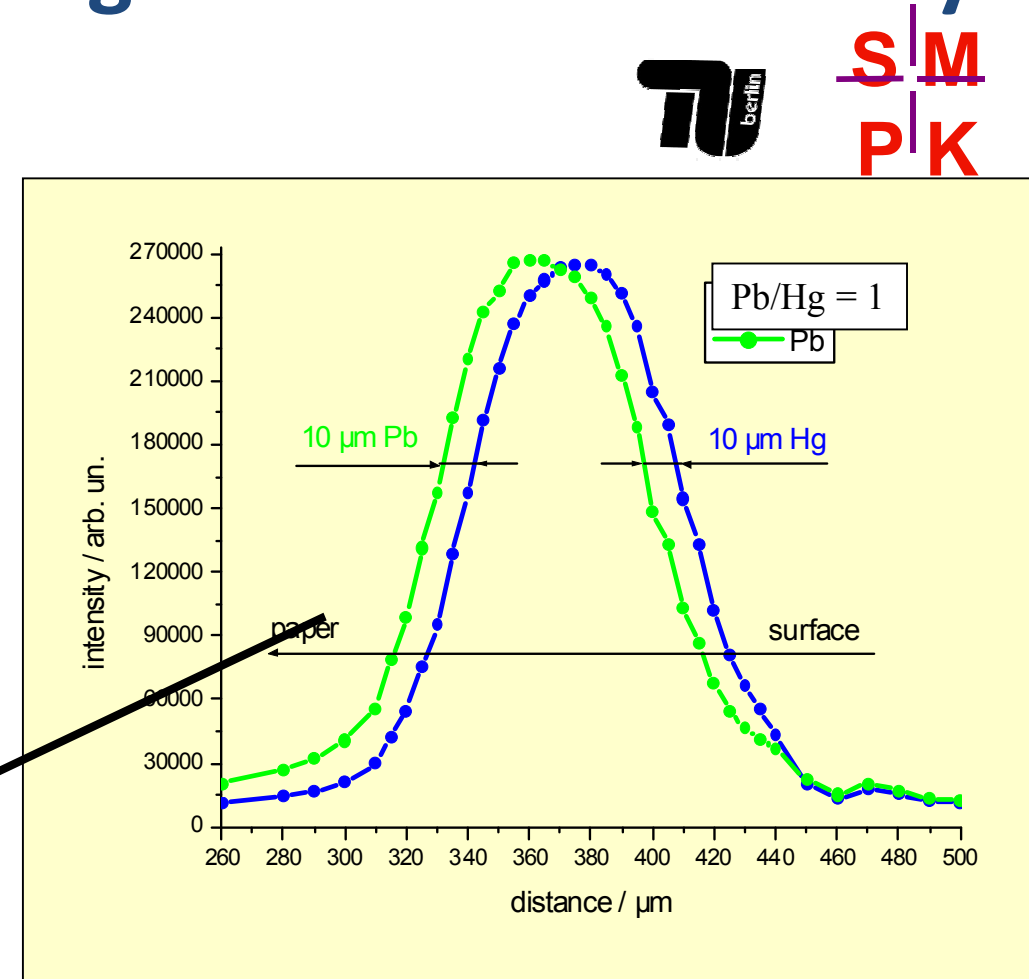
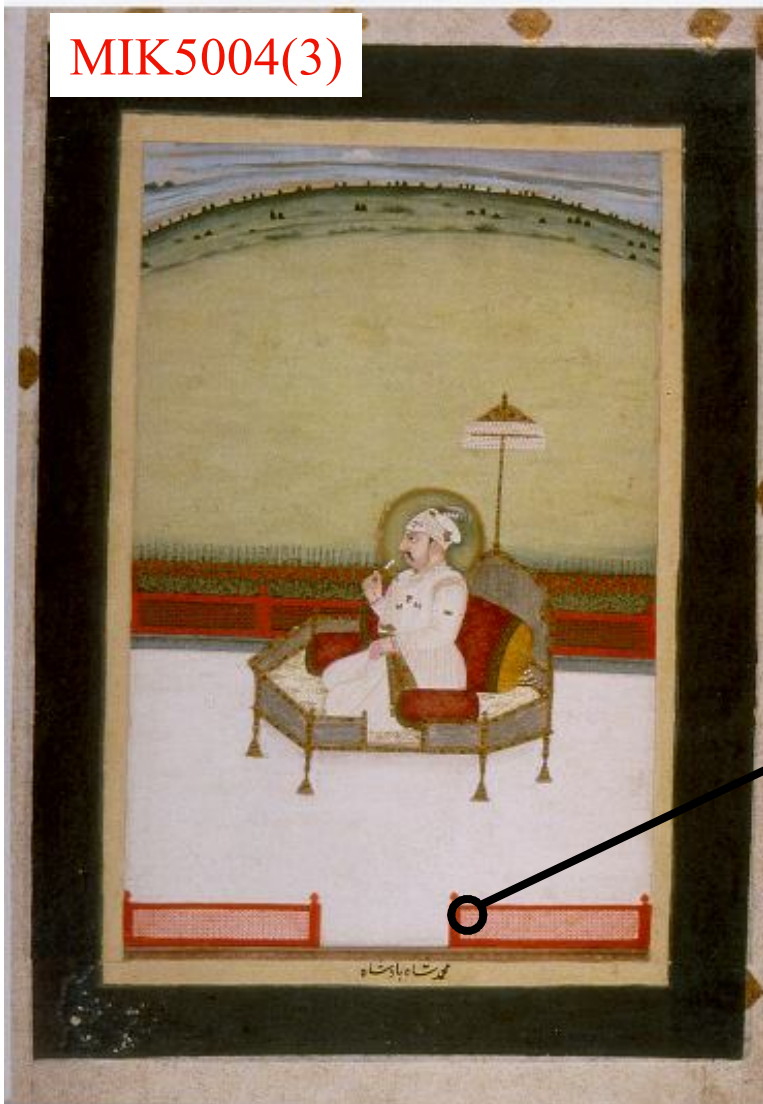
Experimental FWHM, sensitivity/3D uXRF



16, 19 keV excitation energies, Glass Reference materials

I. Mantouvalou, PhD Thesis, Berlin 2009

First 3D Micro-XRF application: Indian Mughal-Paintings 16th – 18th century



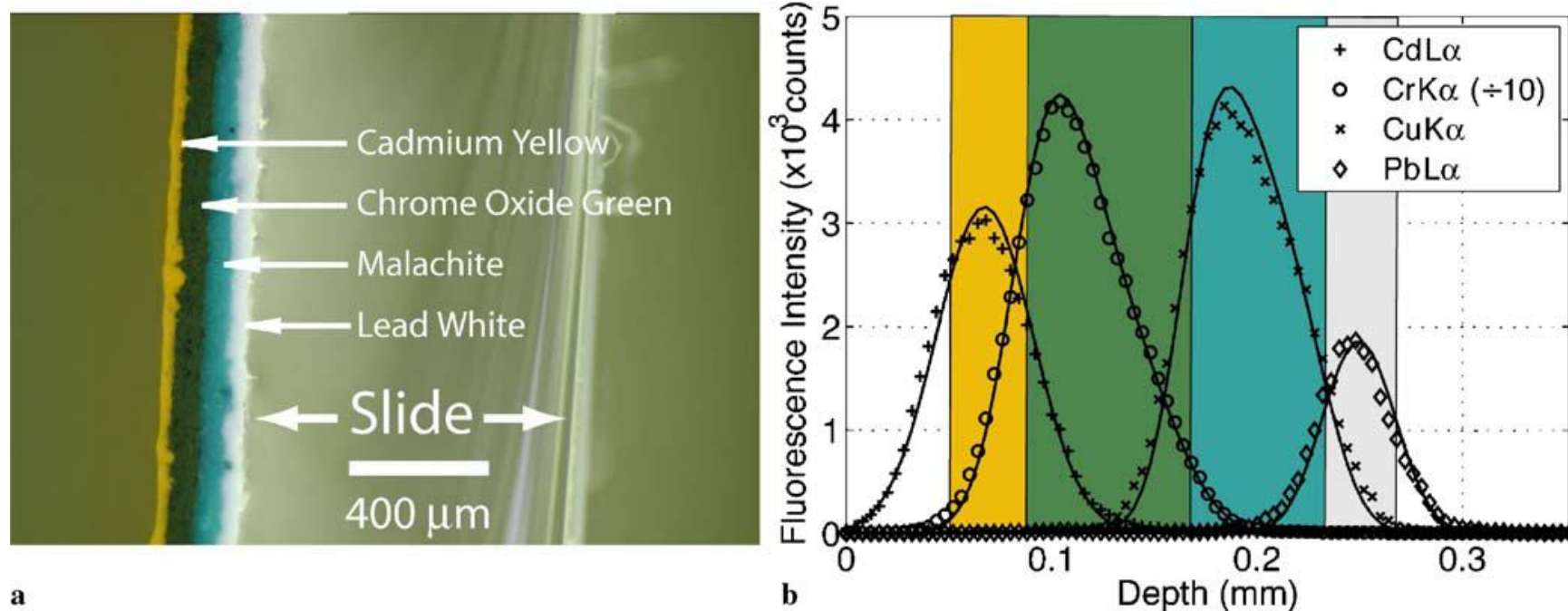
B. Kanngießer, I. Reiche, W. Malzer,
NIM B 211, 2003



IAEA

A.G. Karydas, Joint ICTP-IAEA workshop, November 20, 2014

3D uXRF for Paint layers



Woll et al Appl. Phys. A 83, 235–238 (2006)

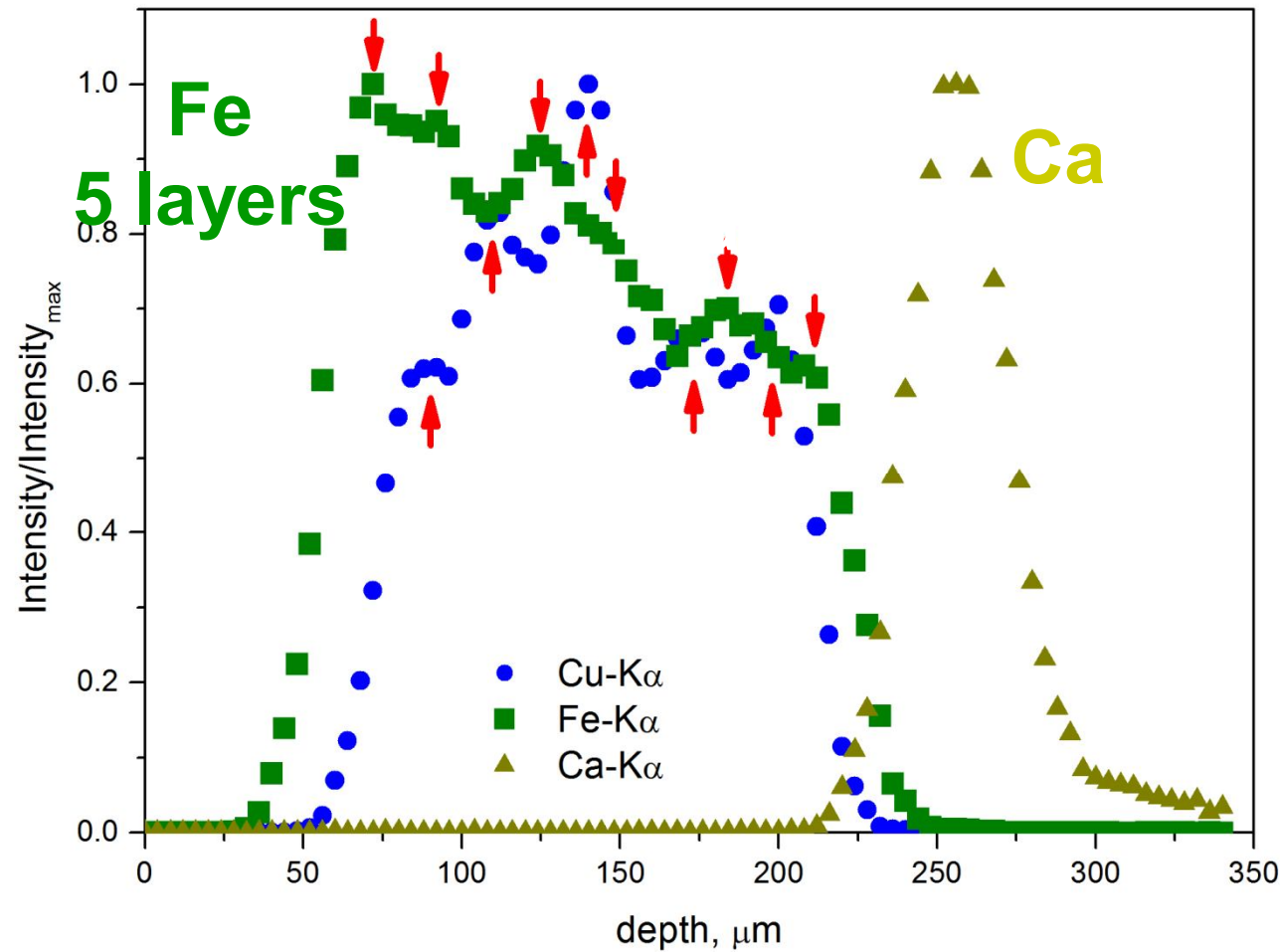
Methodology development: Quantification in 3D Micro-XRF using X-ray tube excitation

Fe/Cu/Fe/Cu/Fe/Cu/Fe/Cu/Fe

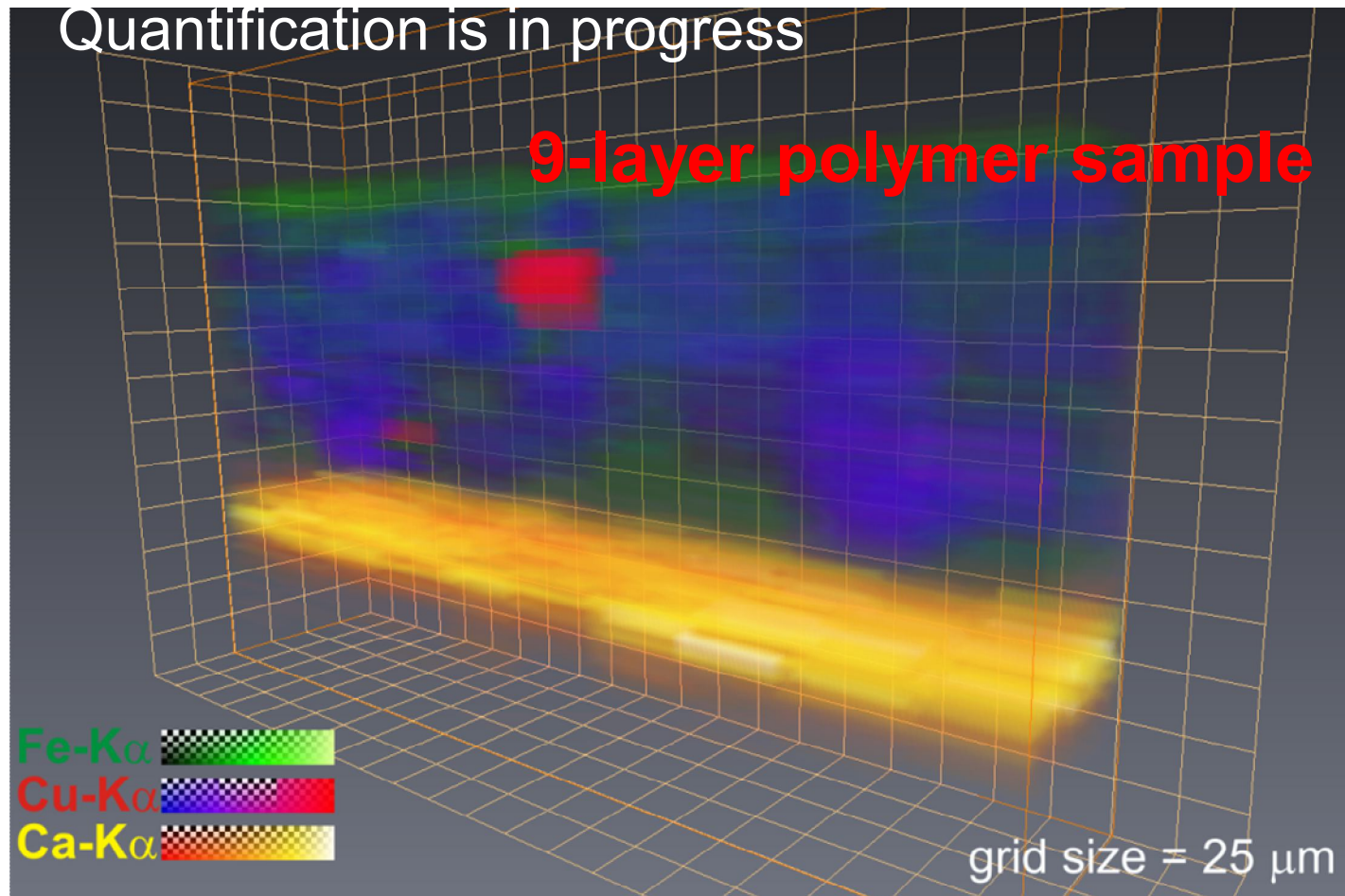
S4:
Multilayer
Polymer
sample
doped with
Fe and Cu



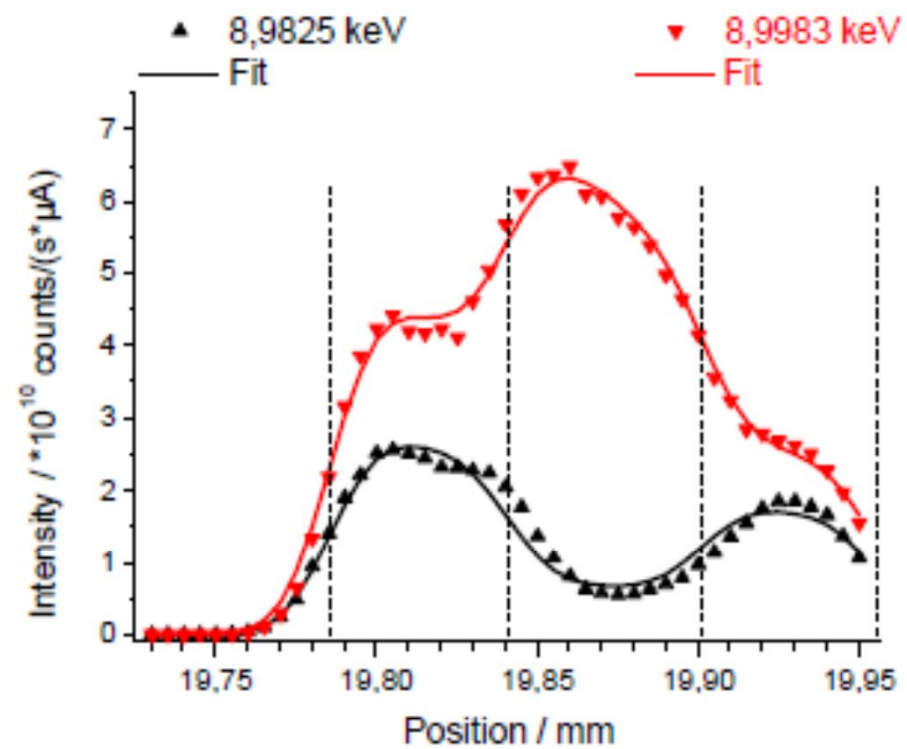
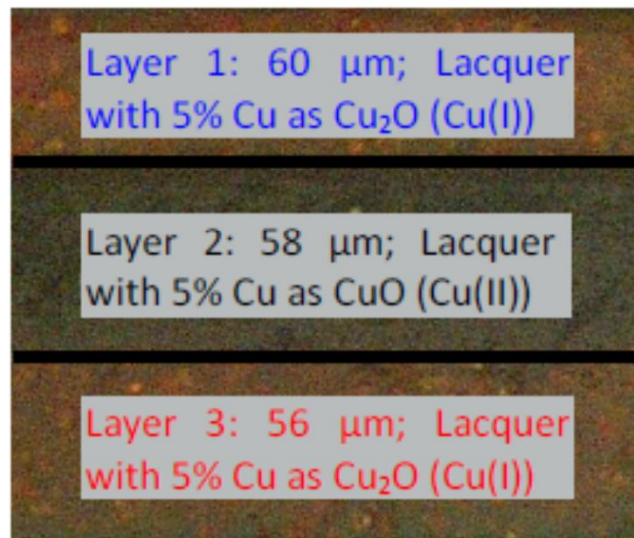
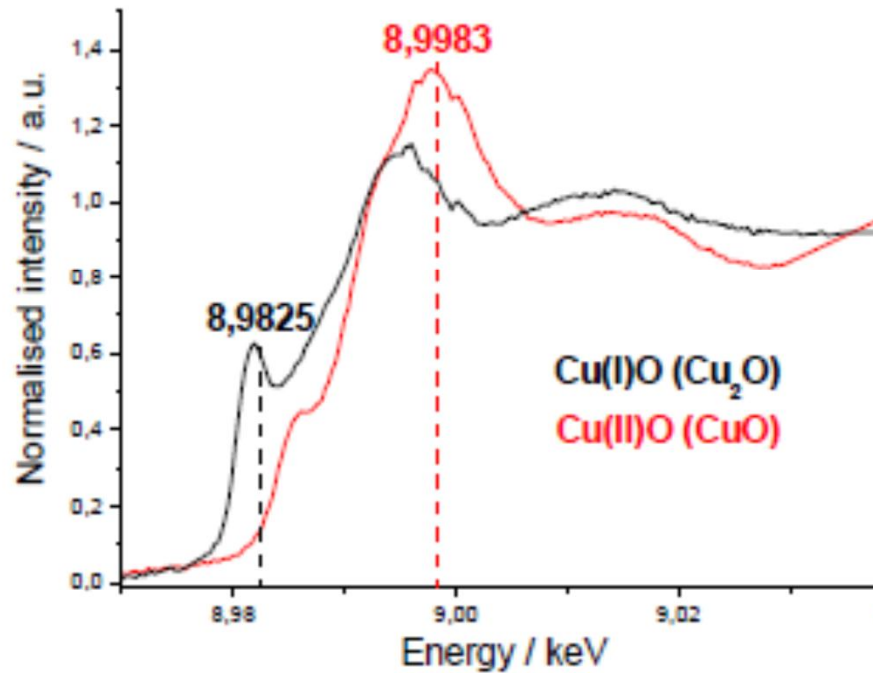
Intensity profiles versus depth



3D Imaging of raw intensity data



3D Chemical mapping with confocal set-up



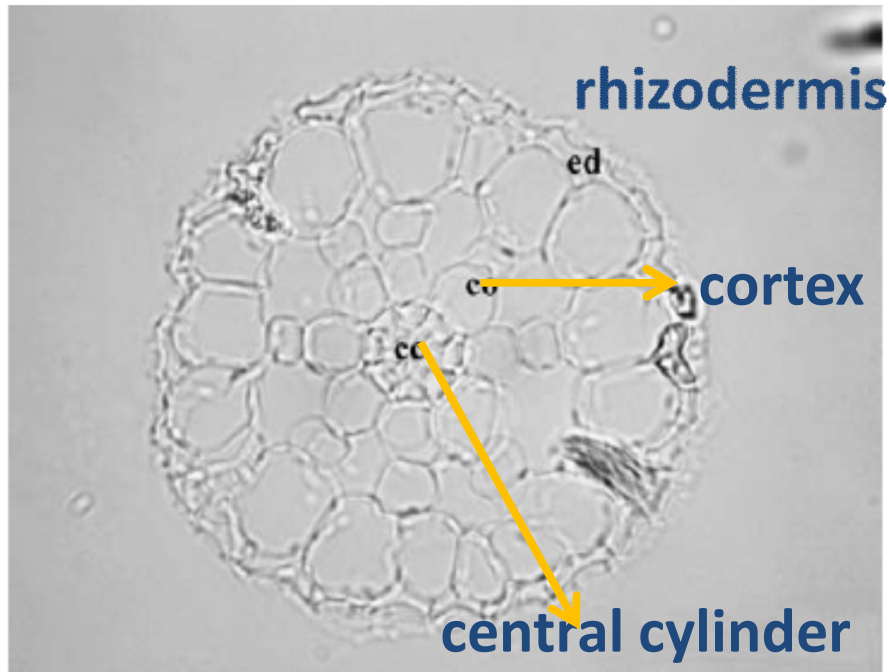
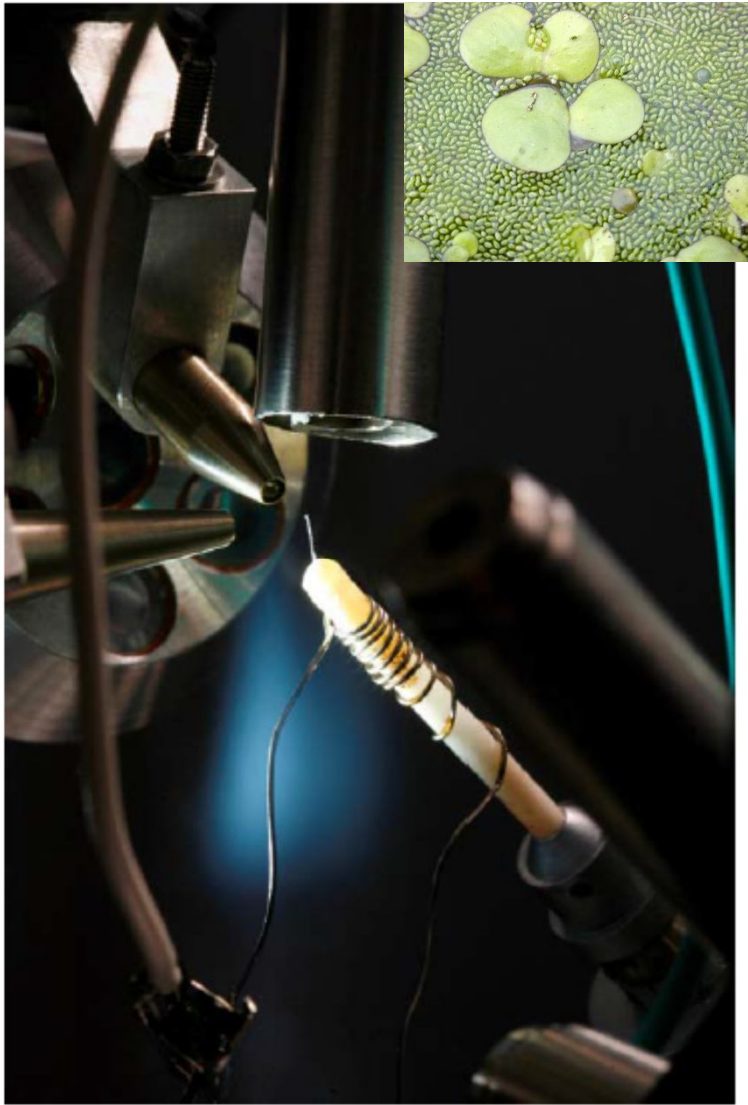
Lars Lühl et al., Three-Dimensional Chemical Mapping with a Confocal XRF Setup, Anal Chem. 2013 Apr 2;85(7):3682-9.



IAEA

A.G. Karydas, Joint ICTP-IAEA workshop, November 20, 2014

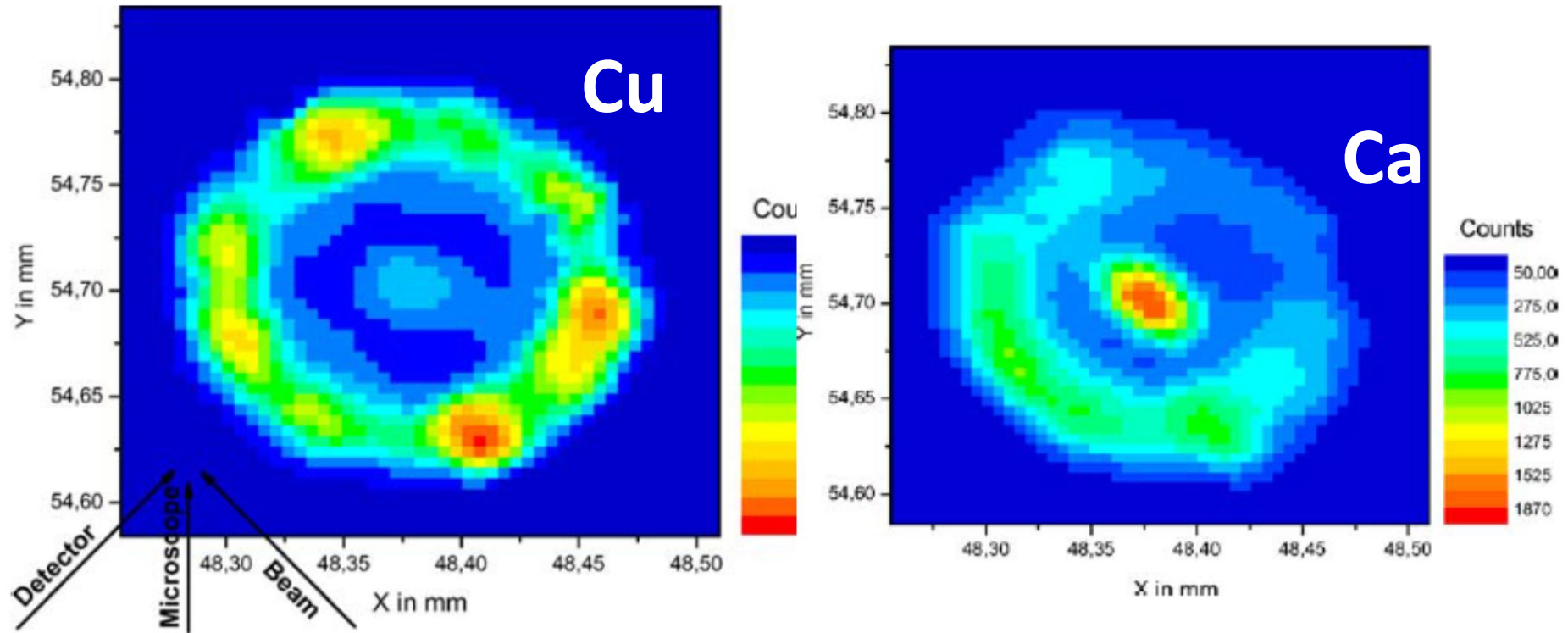
3D Micro-XRF in Biological studies



Kanngiesser et al., Anal Bioanal. Chem. (2007) 389:1171–1176

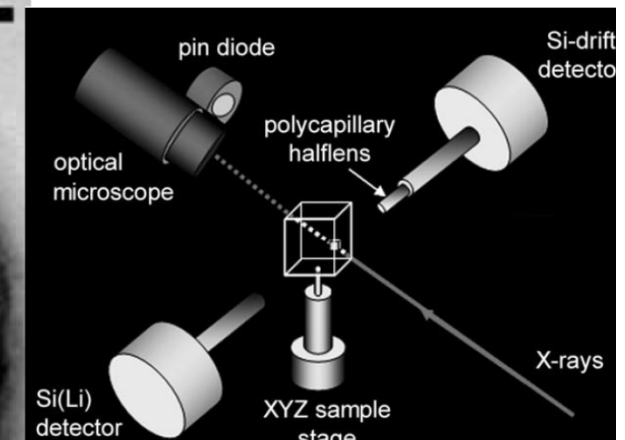
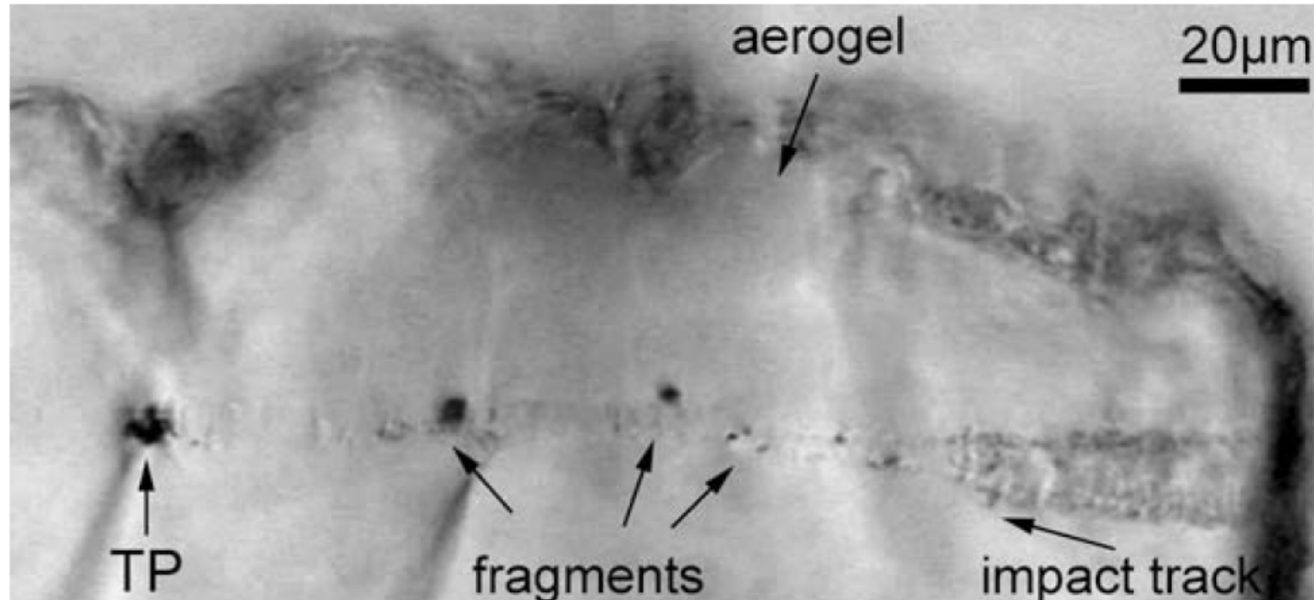
Common duckweed (*Lemna minor*) is an important component of the aquatic food chain. The free floating plant grows on the surface of fresh water ponds and lakes

3D Micro-XRF in Biological studies



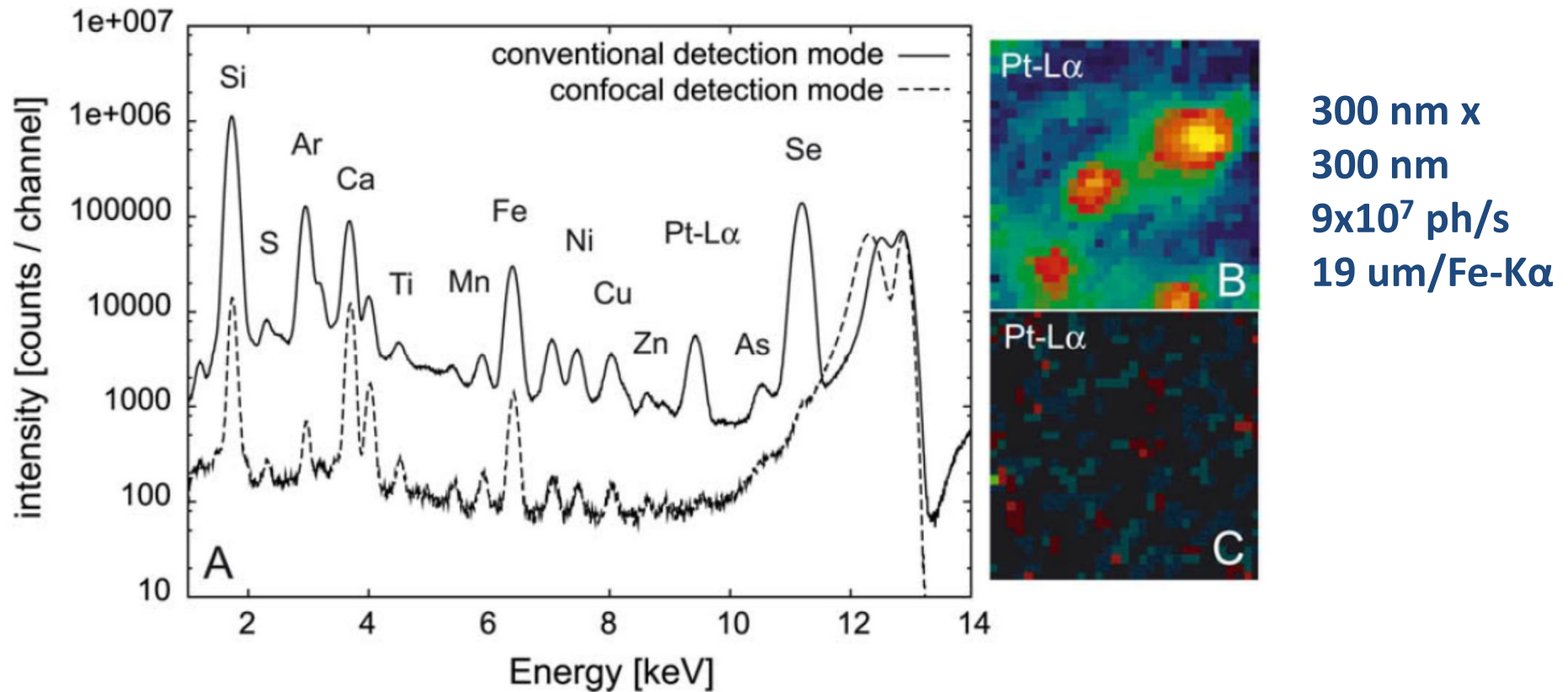
Kanngiesser et al., Anal Bioanal. Chem. (2007) 389:1171–1176

3D Micro-XRF in planetary science

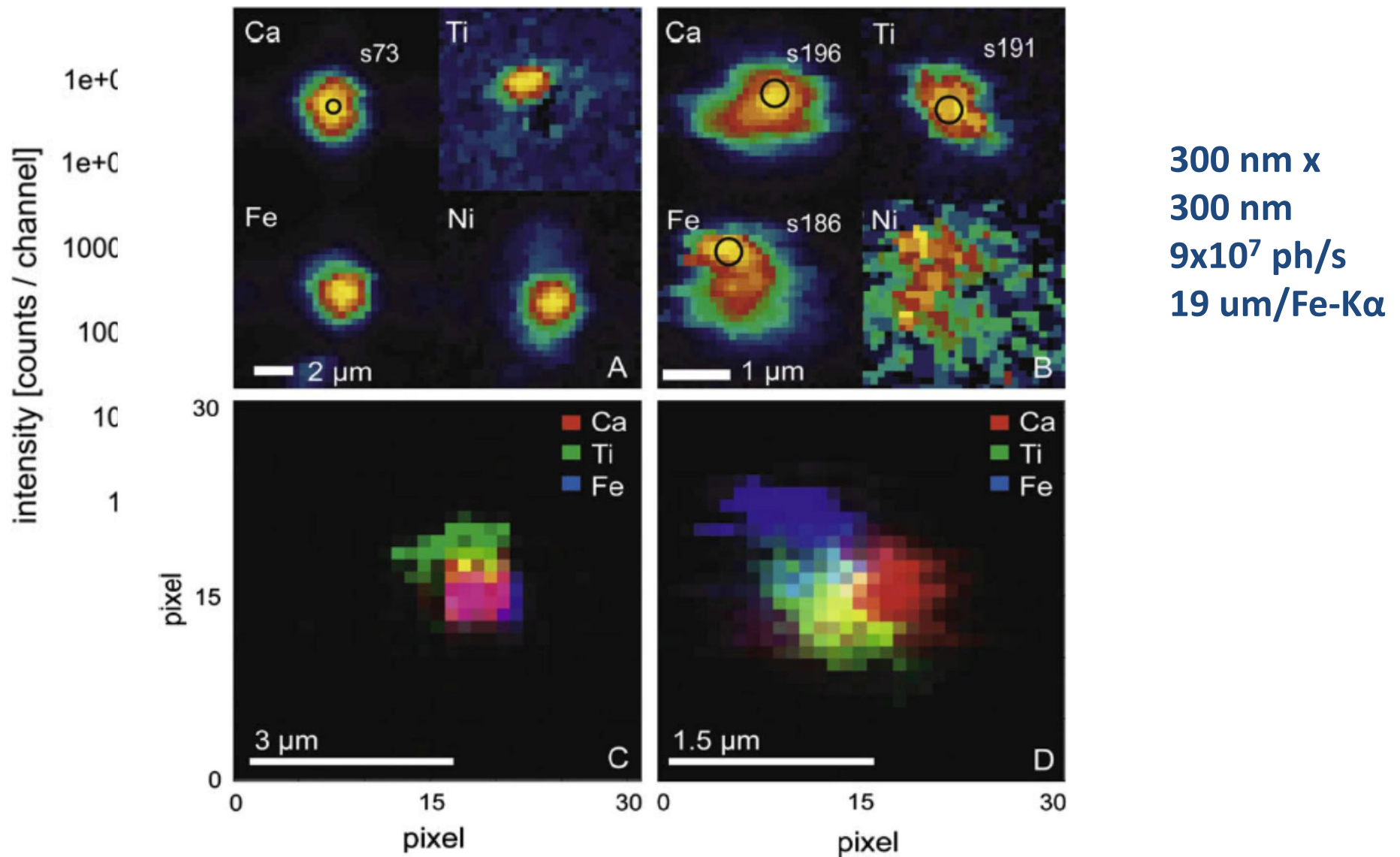


S. Schmitz et al., In situ identification of a CAI candidate in 81P/Wild 2 cometary dust by confocal high resolution synchrotron X-ray fluorescence
Geochimica et Cosmochimica Acta 73 (2009) 5483–5492

3D Micro-XRF in planetary science

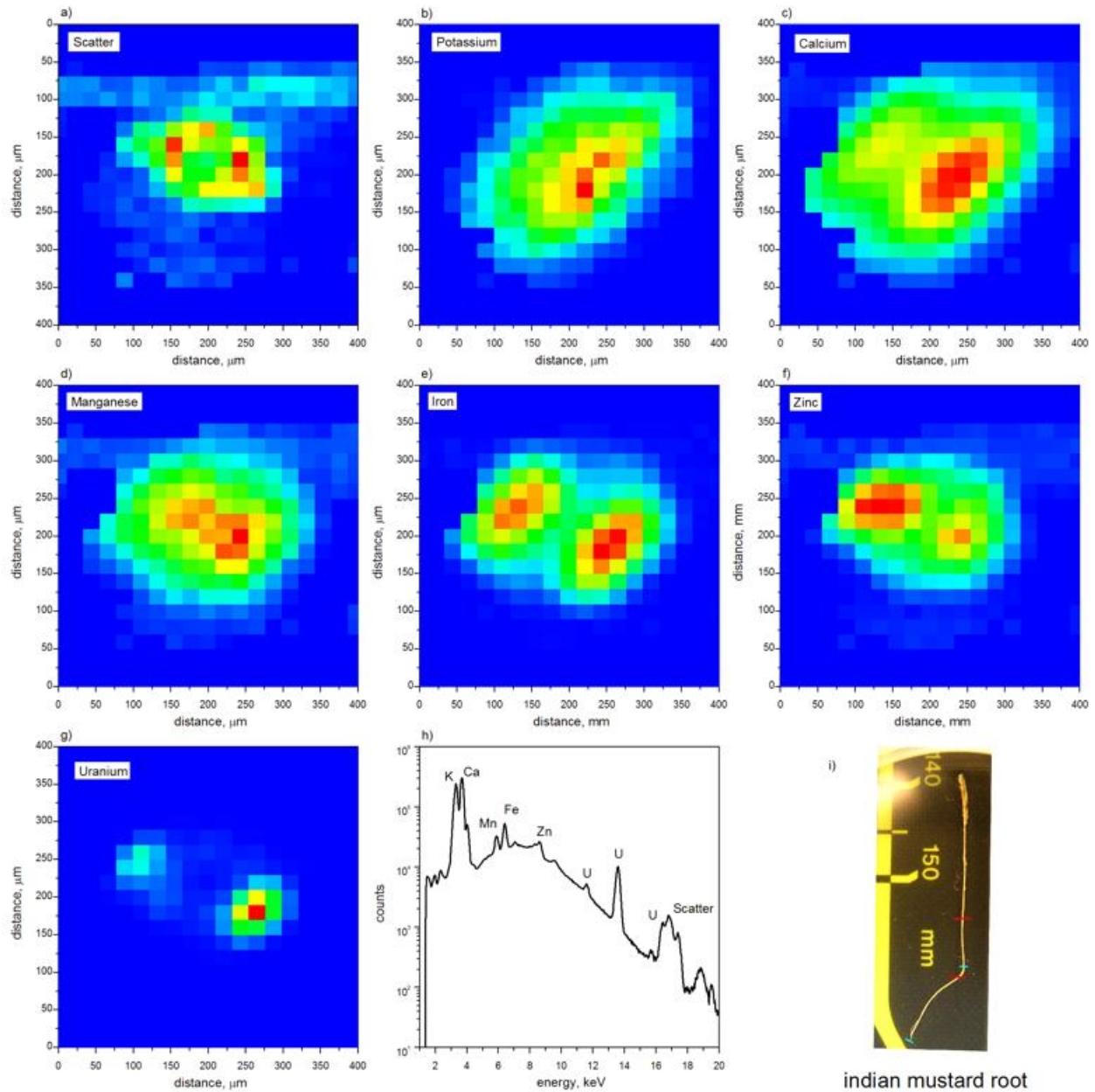


3D Micro-XRF in planetary science

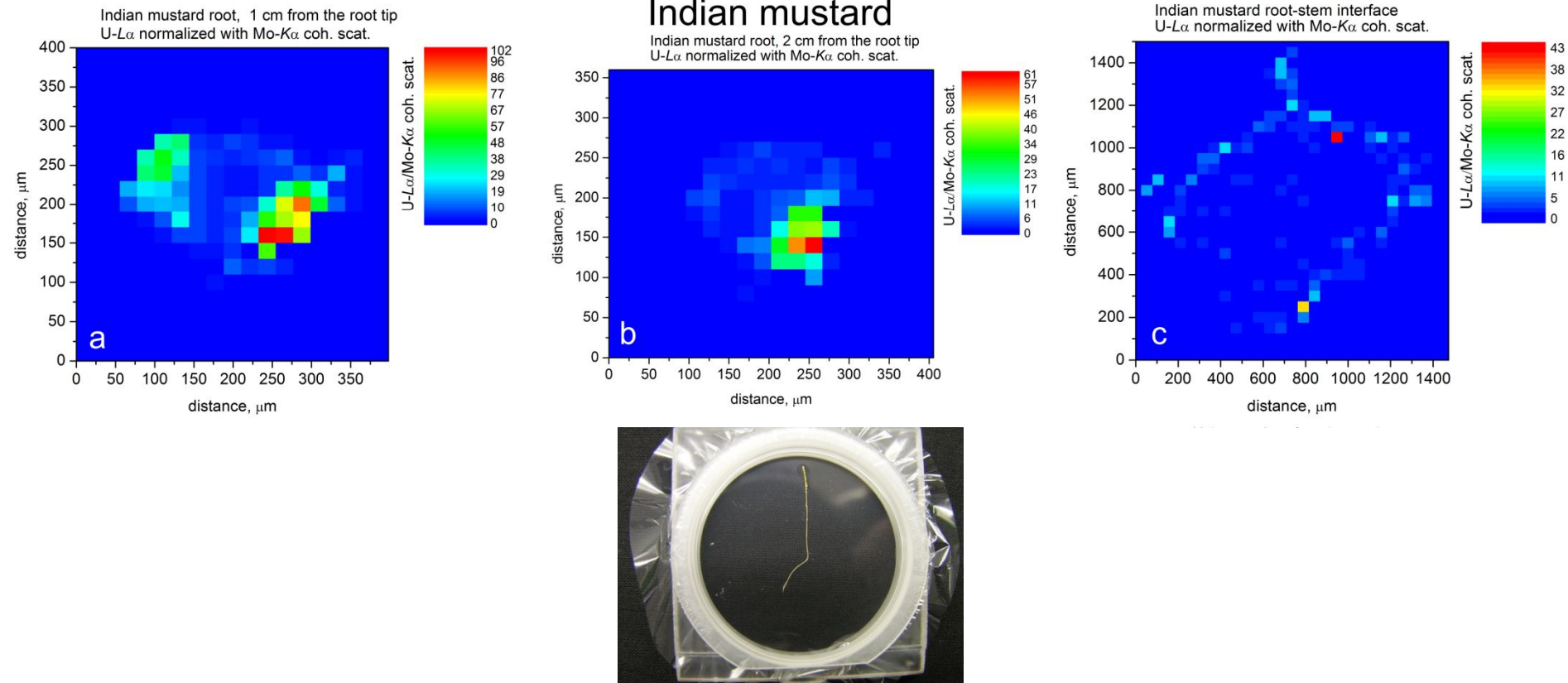


Plant nutrition/transport: Uptake of heavy metals

A. Straczek, et al., J. of Environmental Radioactivity 101(3), 258-266 (2010).

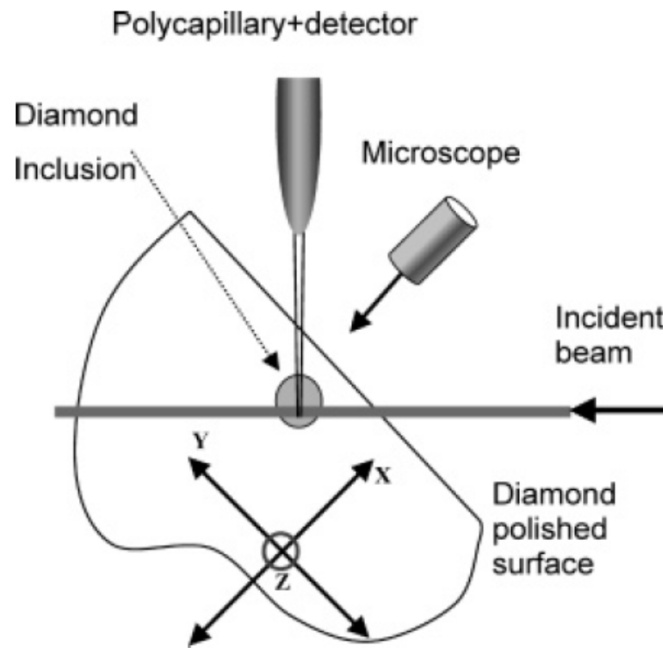


Plant nutrition-transport: Uptake of heavy metals – Uranium



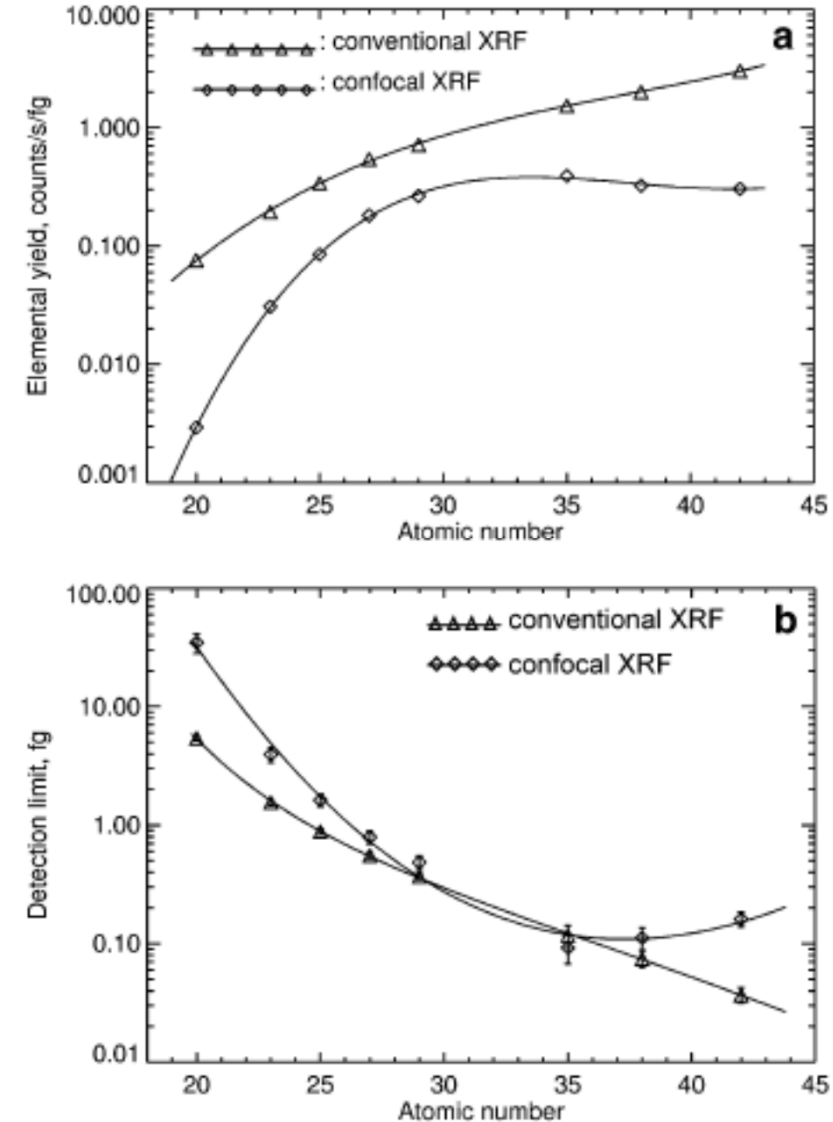
A. Straczek, et al., J. of Environmental Radioactivity 101(3), 258-266 (2010).

3D Micro-XRF applications in Geology

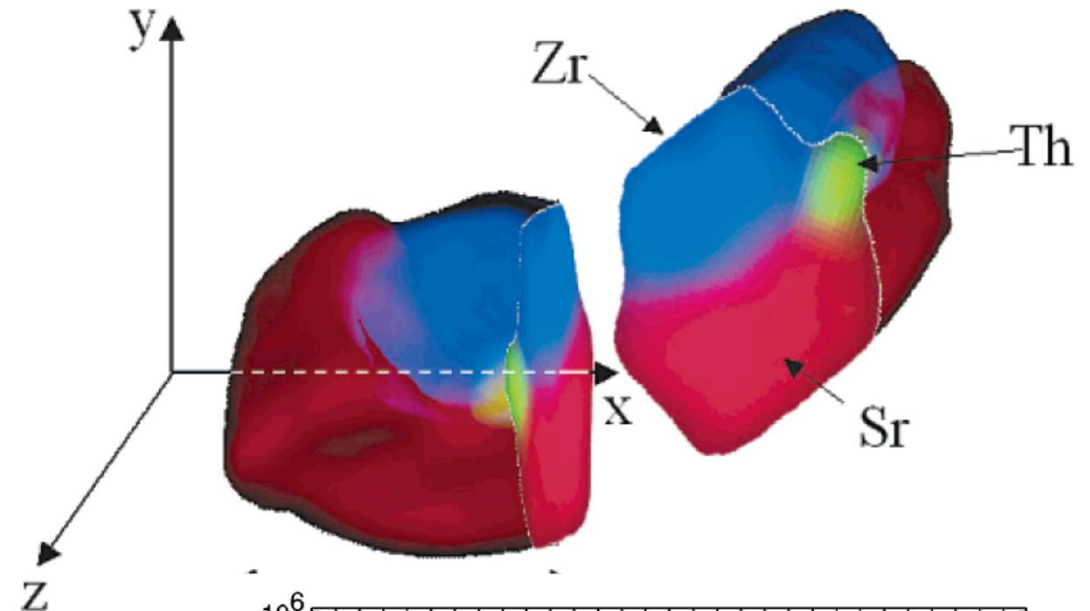
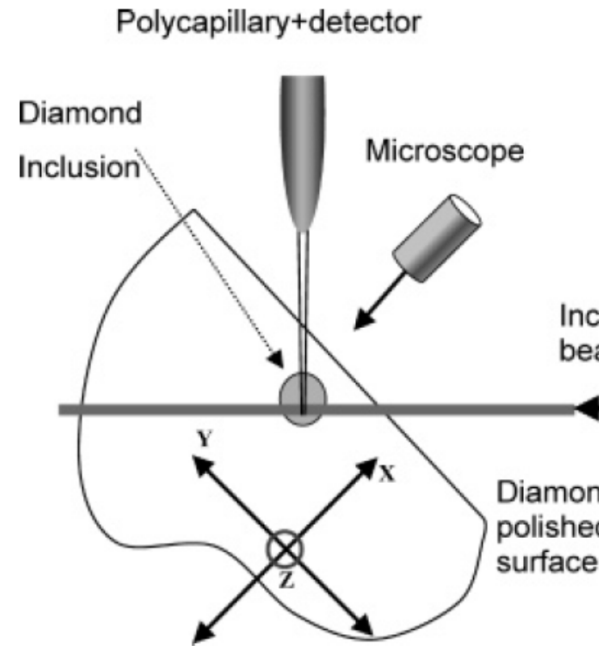


Vincze et al, Anal. Chem.
2004, 76, 6786-6791

28 keV, 2 um (V) X 5 um (H),
 10^{10} photons/s.

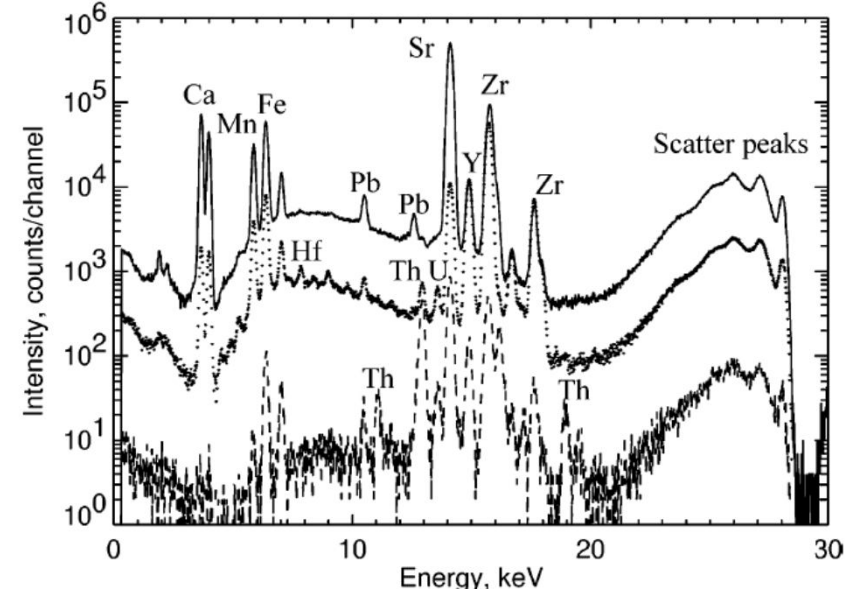


3D Micro-XRF applications in Geology



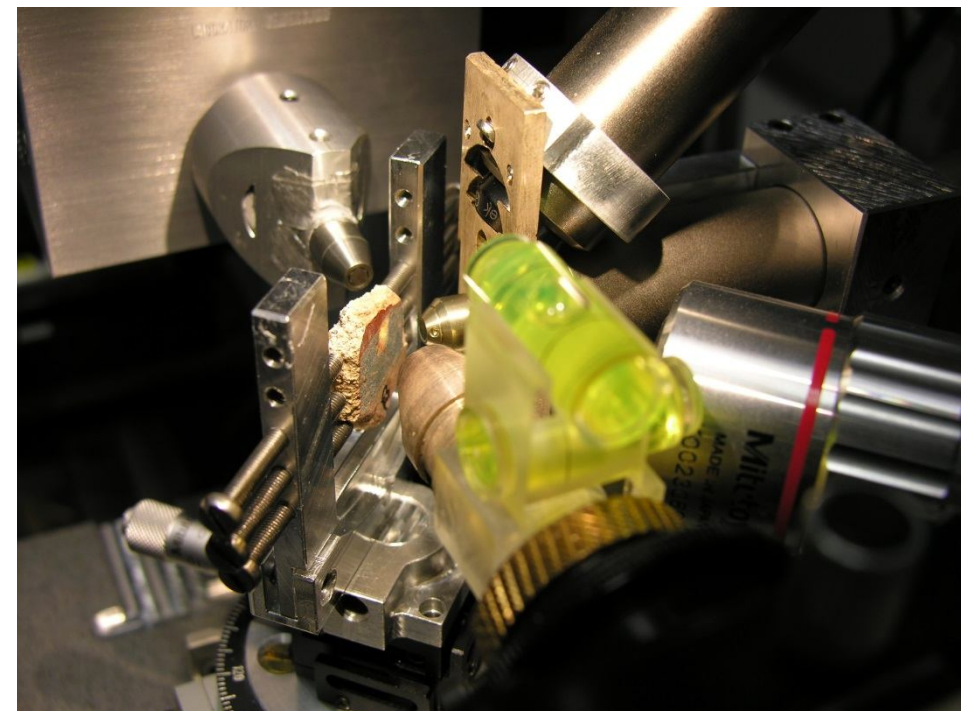
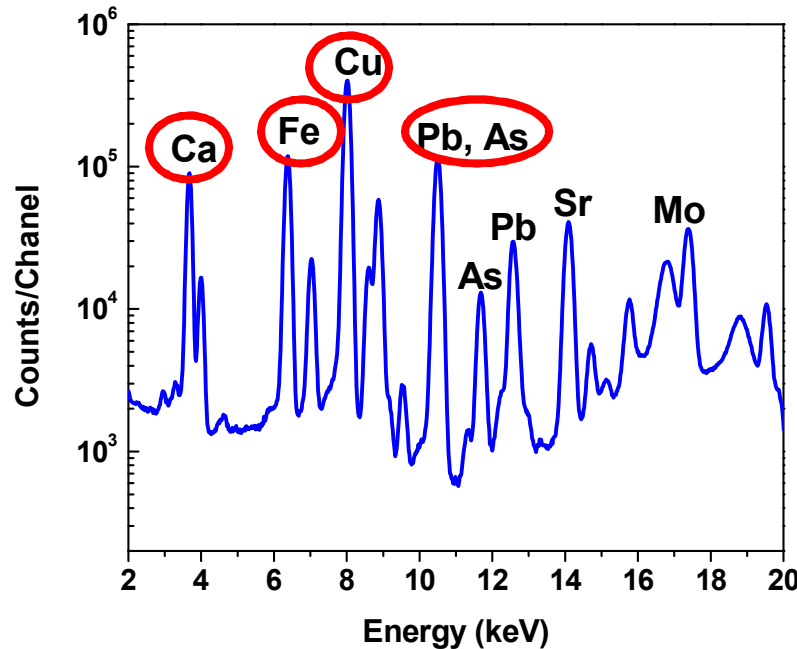
Vincze et al, Anal. Chem.
2004, 76, 6786-6791

28 keV, 2 um (V) X 5 um (H),
 10^{10} photons/s.



3D analysis of Roman period (2 cent BC) painted plasters @IAEA Laboratories

In support of understanding the elaboration of raw materials and application of painting techniques in antiquity.



Micro-XRF spectrum from the analysis on extended area

3D analysis of Roman period (2 cent BC) painted plasters @IAEA Laboratories

Egyptian Blue (Cu)

Red ochre (Fe)

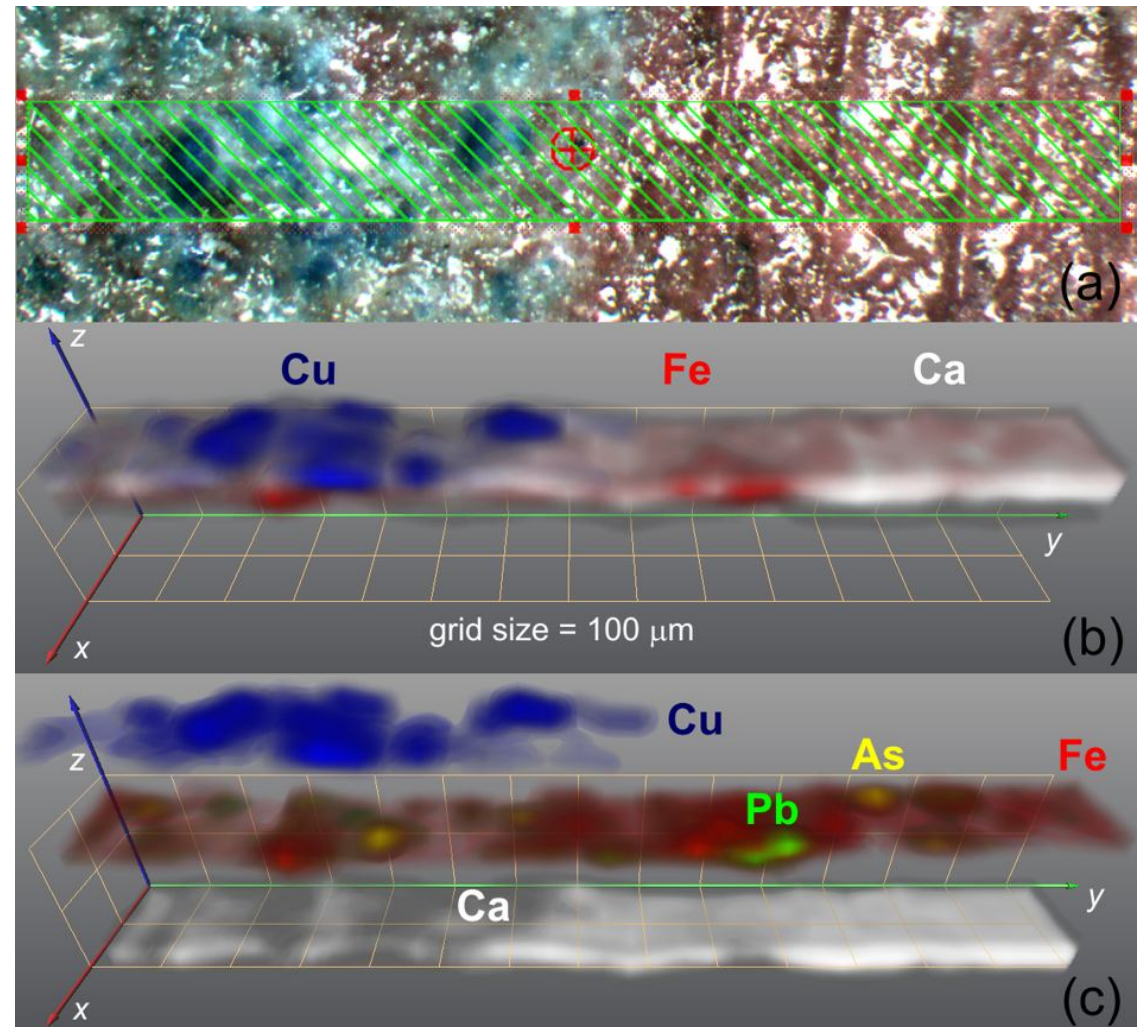
Pb and As are constituents trace-minor elements of the iron based ochre paint layer

Volume:

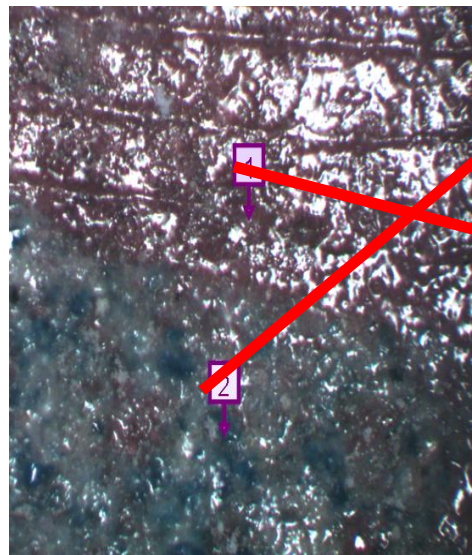
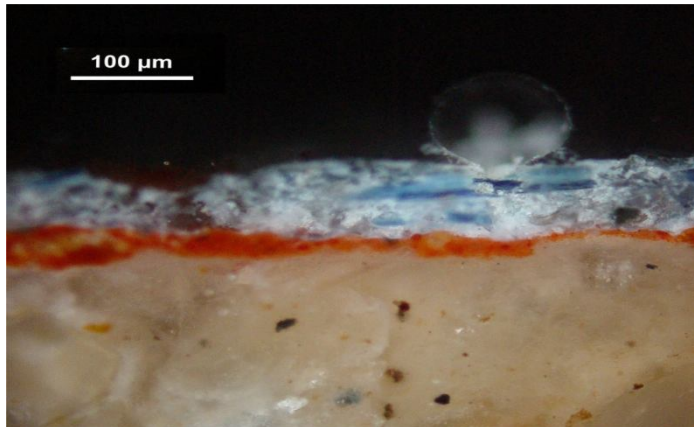
$20 \mu\text{m} \times 1440 \mu\text{m} \times 293 \mu\text{m}$,

xyz scanning spacing:

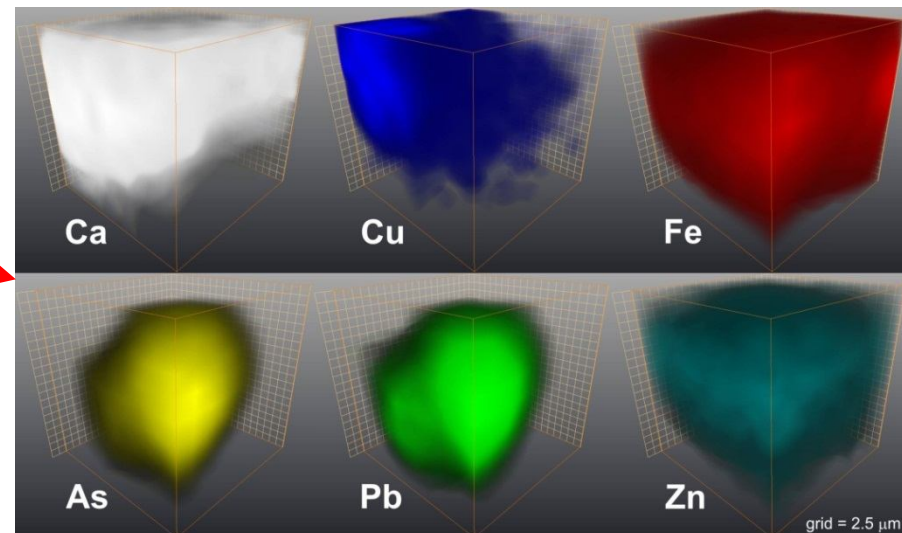
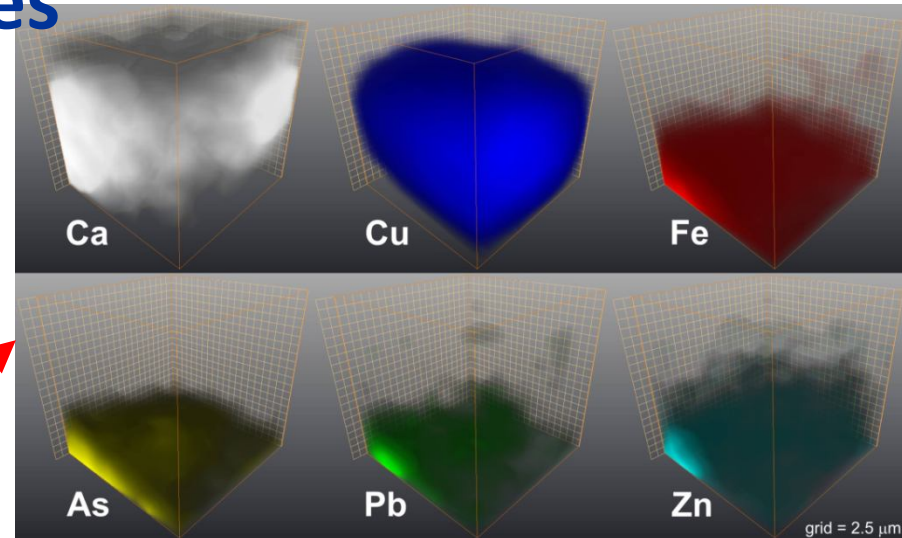
$40 \mu\text{m} \times 40 \mu\text{m} \times 3 \mu\text{m}$



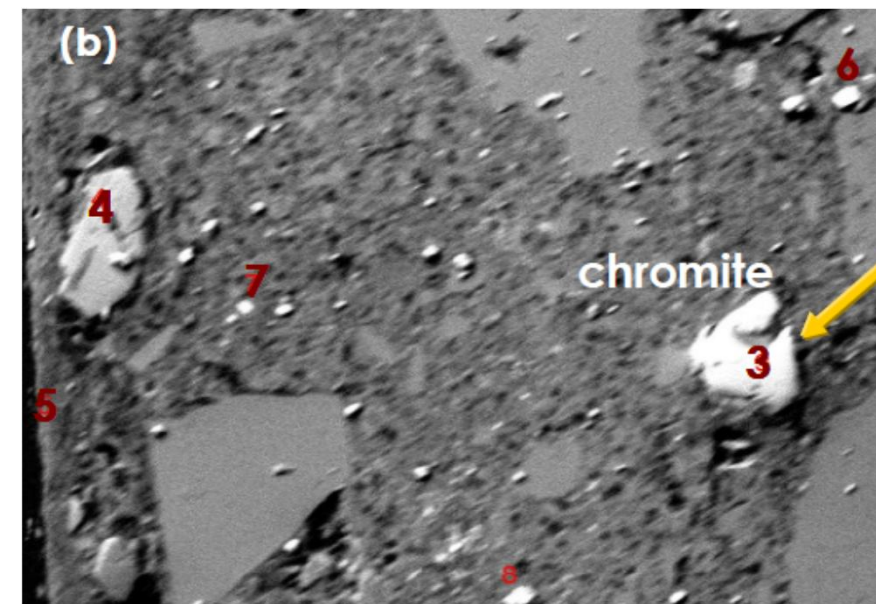
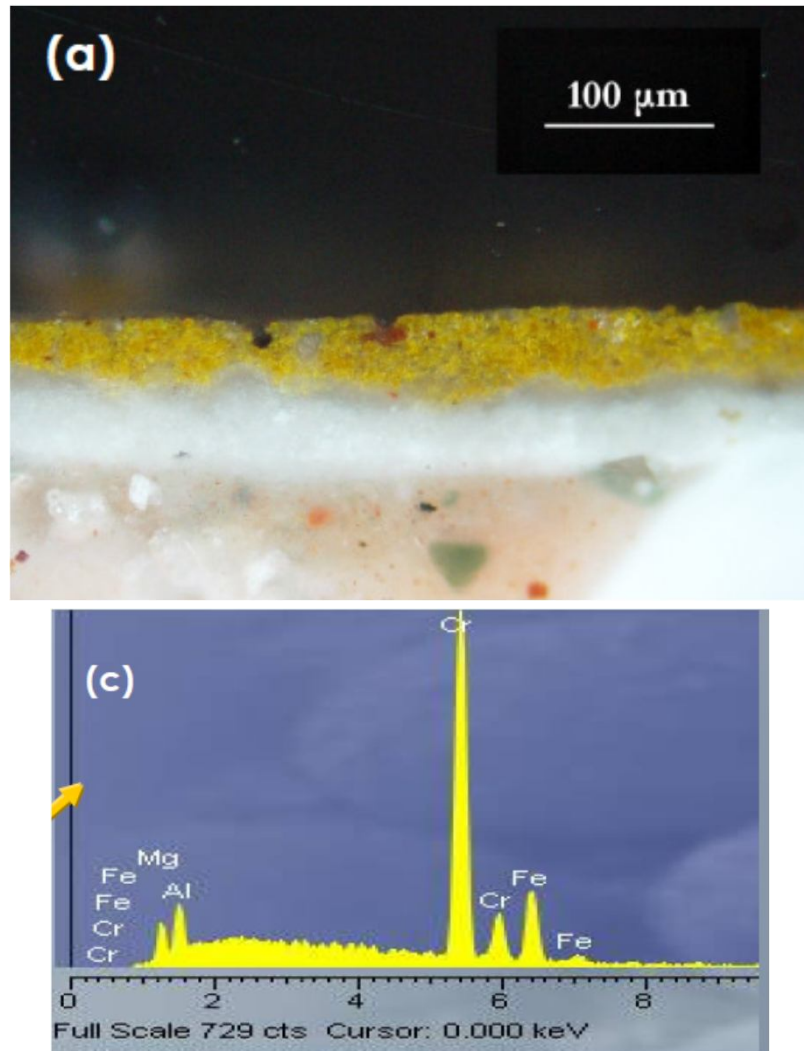
3D analysis of Roman period (2nd cent. BC) painted plasters @IAEA Laboratories



56 μm /55 μm /55 μm
5.6 μm /5.5 μm /5 μm



Identification of minor micro-components

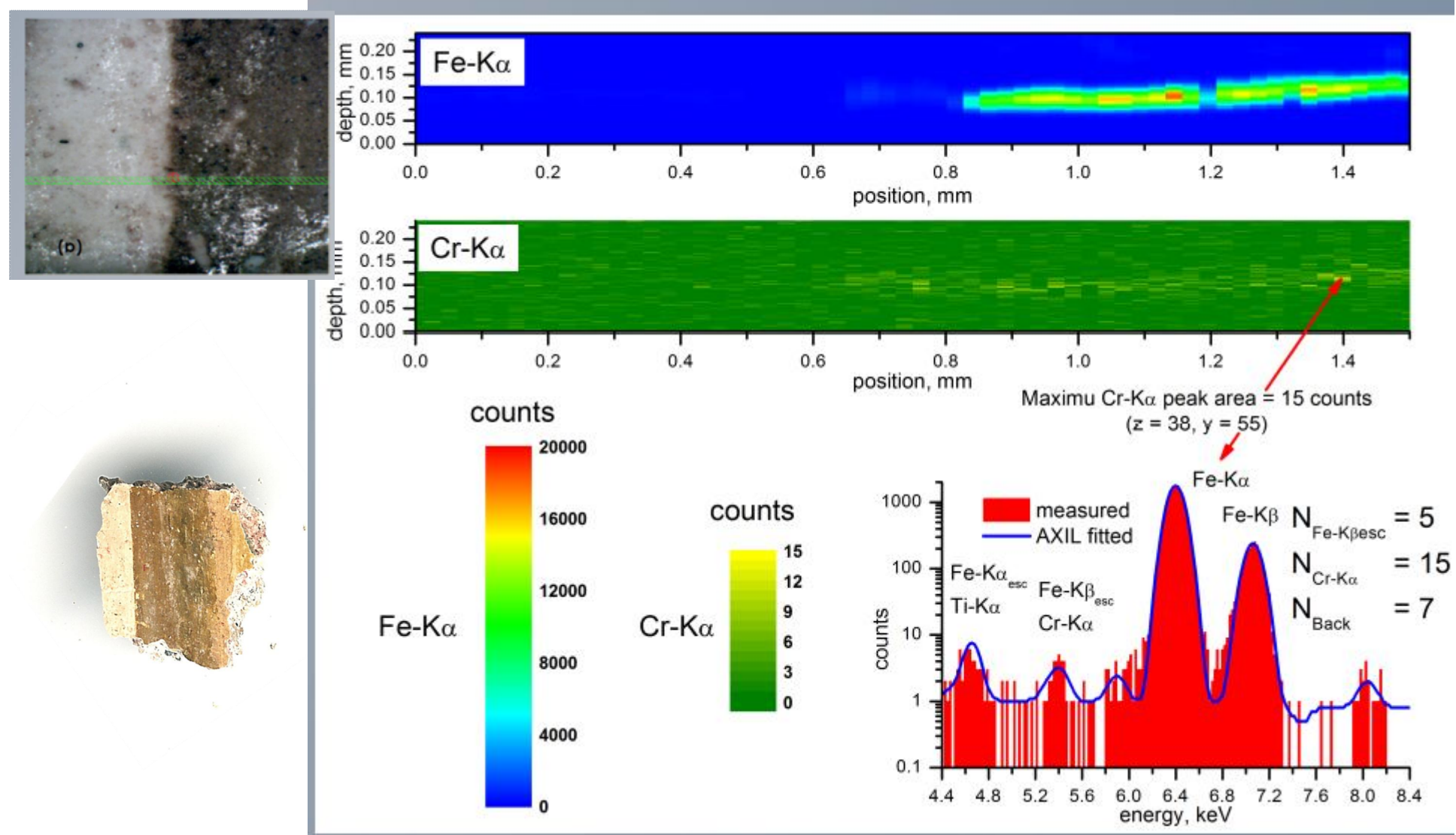


Chromite: $(\text{Mg}, \text{Fe}^{2+})(\text{Cr}, \text{Al})_2\text{O}_4$

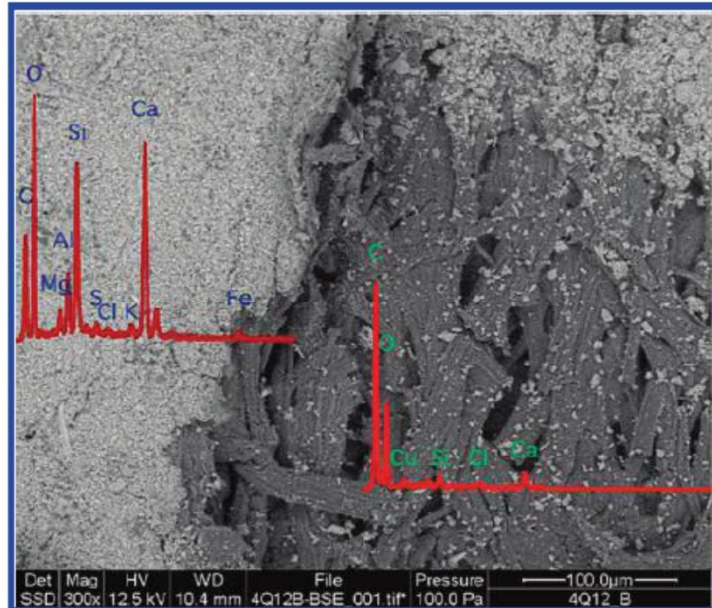
Collaboration with Technical University of Crete and National Research Foundation – KERAS

Samples: courtesy by H. Brecoulaki, KERAS

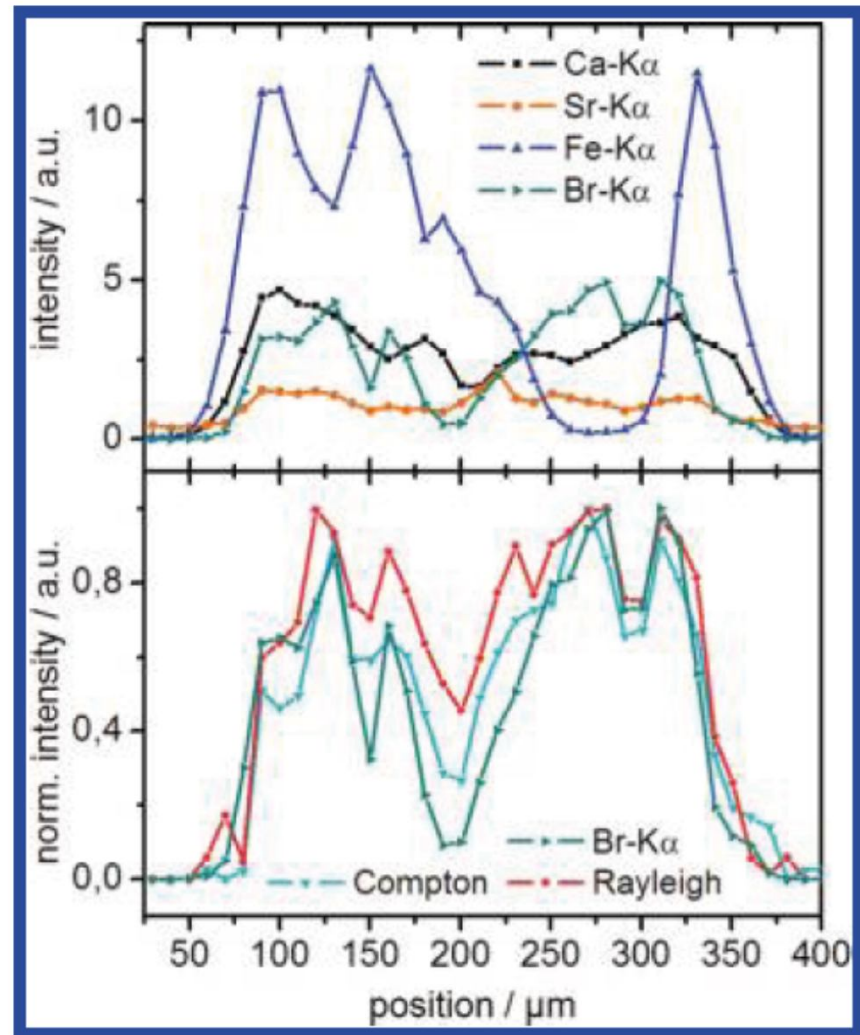
Identification of minor micro-components



Combined 3D Micro-XRF/2D Micro XRF on the Dead Sea Scrolls



Mantouvalou et al Anal. Chem. 2011,
83, 6308–6315



Synopsis/Complementarily

Elements (Alumino-silicate matrix)	Techniques	Probing Depth	Concentration
Na - Cl	3D Micro -PIXE	<10-20 µm	Major
K-Zn	3D Micro -PIXE 3D Micro -XRF	<100 µm	Major/Minor Major/Minor
Ga – Ag, Au-U Ga - U	3D Micro –PIXE 3D Micro -XRF	<100 µm 100-300 µm	Major Major/Minor/Trace

Synopsis

- The intensity profiles deduced from confocal depth scans incorporate composite analytical information such as the position and height of its centroid, the fwhm or actually the exact shape of the intensity distribution.
3D analysis may offer various analytical possibilities:
 - ✓ To resolve the features of a multilayered structure (elemental composition, thickness, layers)
 - ✓ To estimate concentration gradients
 - ✓ Elemental composition of few tens um scale particles embedded mostly in a light matrix

Thank you for your attention!!

Acknowledgements

D. Wegrzynek, R. Padilla-Alvarez,
Ch. Apostolaki, Ch. Brecoulaki,
TUB group and B. Kanngiesser